Overlap valence on 2 + 1 flavor domain wall fermion configurations with deflation and low-mode substitution

A. Li (李安意),[1,2] A. Alexandru,[3] Y. Chen,[4] T. Doi,[5] S. J. Dong,[2] T. Draper,[2] M. Gong (宫明),[2] A. Hasenfratz,[6] I. Horváth,[2] F. X. Lee,[3] K. F. Liu (刘克非),[2] N. Mathur,[7] T. Streuer,[8] and J. B. Zhang[9]

[1]*Department of Physics, Duke University, Durham, North Carolina 27708, USA*
[2]*Department of Physics and Astronomy, University of Kentucky, Lexington, Kentucky 40506, USA*
[3]*Department of Physics, George Washington University, Washington, D.C. 20052, USA*
[4]*Institute of High Energy Physics, Chinese Academy of Science, Beijing 100049, China*
[5]*Graduate School of Pure and Applied Science, University of Tsukuba, Tsukuba, Ibaraki 305-8571, Japan*
[6]*Department of Physics, University of Colorado, Boulder, Colorado 80309, USA*
[7]*Department of Theoretical Physics, Tata Institute of Fundamental Research, Mumbai 40005, India*
[8]*Institute for Theoretical Physics, University of Regensburg, 93040 Regensburg, Germany*
[9]*ZIMP and Department of Physics, Zhejiang University, Hangzhou, Zhejiang 310027, China*

The overlap fermion propagator is calculated on 2 + 1 flavor domain-wall fermion gauge configurations on $16^3 \times 32$, $24^3 \times 64$ and $32^3 \times 64$ lattices. With hyper-cubic (HYP) smearing and low eigenmode deflation, it is shown that the inversion of the overlap operator can be expedited by ~ 20 times for the $16^3 \times 32$ lattice and ~ 80 times for the $32^3 \times 64$ lattice. The overhead cost for calculating eigenmodes ranges from 4.5 to 7.9 propagators for the above lattices. Through the study of hyperfine splitting, we found that the $O(m^2 a^2)$ error is small and these dynamical fermion lattices can adequately accommodate quark mass up to the charm quark. A preliminary calculation of the low-energy constant Δ_{mix} which characterizes the discretization error of the pion made up of a pair of sea and valence quarks in this mixed-action approach is carried out via the scalar correlator with periodic and antiperiodic boundary conditions. It is found to be small which shifts a 300 MeV pion mass by ~ 10 to 19 MeV on these sets of lattices. We have studied the signal-to-noise issue of the noise source for the meson and baryon. We introduce a new algorithm with Z_3 grid source and low eigenmode substitution to study the many-to-all meson and baryon correlators. It is found to be efficient in reducing errors for the correlators of both mesons and baryons. With 64-point Z_3 grid source and low-mode substitution, it can reduce the statistical errors of the light quark ($m_\pi \sim 200$–300 MeV) meson and nucleon correlators by a factor of ~ 3–4 as compared to the point source. The Z_3 grid source itself can reduce the errors of the charmonium correlators by a factor of ~ 3.

I. INTRODUCTION

A large scale endeavor has been undertaken by the RBC and UKQCD collaborations in the last few years to simulate 2 + 1 flavor full QCD with dynamical domain-wall fermions (DWF) and Iwasaki gauge action on several lattices with pion mass as low as ~ 300 MeV and volume large enough for mesons ($m_\pi L > 4$) [1–3]. Three sets of lattices $16^3 \times 32 \times L_S$ and $24^3 \times 64 \times L_S$ at $a^{-1} = 1.73(3)$ GeV and $32^3 \times 64 \times L_S$ at $a^{-1} = 2.32(3)$ GeV with the fifth dimension $L_S = 16$ are available, each with 3 to 4 sea quark masses with the lowest pion mass at ~ 300 MeV. With these lattices, one can proceed to perform chiral extrapolation and continuum extrapolation assuming a^2 dependence of the physical quantities. Since the domain-wall fermion with $L_S = 16$ is a good approximation for the chiral fermion satisfying Ginsparg-Wilson relation, it is shown that they have good chiral properties and that most of the chiral symmetry breaking effects are absorbed in the residual mass which is reasonably small for these set of lattices. As such, these dynamical fermion configurations are very valuable and can be used to calculate physical quantities reliably, at least for the mesons. It is suggested from the study of the nucleon axial coupling g_A and electromagnetic form factors that the present lattices are still small and lattices with spatial dimension of 6 fm might be needed in order to control the finite volume errors.

While combined chiral extrapolation and continuum extrapolation are being carried out with valence domain-wall fermions, we shall explore the viability of employing valence overlap fermions on these DWF configurations. Both the domain-wall fermion and the overlap fermion are chiral fermions. As such, they do not have $O(a)$ errors and non-perturbative renormalization via chiral Ward identities or the regularization independent/momentum subtraction (RI/MOM) scheme can be implemented relatively easily [4–6]. Furthermore, the overlap fermion has additional desirable features which one can take advantage of in order to improve chiral symmetry as well as the quality of the numerical results. First of all, the numerical implementation of the overlap fermion allows a precise approximation of the matrix sign function so that the errors on the sign function and thus

the residual mass can be as small as 10^{-10} in practice [7]. The approximation to the exact chiral symmetry can also be gauged from the Ginsparg-Wilson and the Gell-Mann-Oakes-Renner relations. Its multimass algorithm permits calculation of multiple quark propagators covering the range from very light quarks to the charm on these sets of DWF lattices. This makes it possible to include the charm quark for calculations of charmonium and charmed-light mesons using the same fermion formulation for the charm and light quarks [8]. It is also possible to incorporate partially quenched data in the chiral extrapolation. Since the overlap operator is a normal matrix, it is easier to calculate its eigenmodes and implement low-mode deflation in the matrix inversion. As we shall see, this can speed up the inversion of small quark mass by more than an order of magnitude with no critical slowing down. Furthermore, these low-frequency modes can be used together with the noise approximation of the high-frequency modes to construct all-to-all or many-to-all correlators. We shall show that using Z_3 grid source on a time slice is quite efficient in reducing variance for both the meson and baryon correlators. We should point out that although both the overlap and domain-wall fermions are chiral fermions, using overlap valence on DWF gauge configurations with HYP smearing at finite lattice spacing constitutes a mixed-action approach. Mixed-action approaches have been studied by many groups such as DWF valence on staggered fermion sea [9], overlap valence on DWF sea [10], overlap valence on clover sea [11], and overlap valence on twisted fermion sea [12]. It is shown that the valence chiral fermion has the advantage that it introduces only one extra low-energy constant Δ_{mix} in the mass of the pseudoscalar meson with mixed valence and sea quarks which has the same effect as partial quenching. The mixed-action partially quenched chiral perturbation theory (MAPQχPT) which has been worked out for various physical quantities with various combination of fermion actions will be the simplest for the combination of overlap valence and DWF sea.

This manuscript is organized as follows: The formalism for solving linear equation of the overlap operator with low eigenmode deflation and Z_3 noise grid for the many-to-all correlators will be given in Sec. II. The numerical details on the tuning of the negative mass parameter ρ in the Wilson kernel of the overlap, the speedup due to HYP smearing and low-mode deflation, and the role of the zero mode will be presented in Sec. III. In Sec. IV, we shall present the calculation of Δ_{mix} and results for the meson and nucleon correlators with point source, Z_3 grid source, and Z_3 grid source with low-mode substitution. The efficacy of the many-to-all approach will be discussed. We will finish with a summary in Sec. V.

II. FORMALISM

The massless overlap operator [13] is defined as

$$D_{\mathrm{ov}}(\rho) = 1 + \gamma_5 \epsilon(H_W(\rho)), \qquad (1)$$

where $\epsilon(H_W) = H_W/\sqrt{H_W^2}$ is the matrix sign function and H_W is taken to be the Hermitian Wilson-Dirac operator, i.e. $H_W(\rho) = \gamma_5 D_W(\rho)$. Here $D_w(\rho)$ is the usual Wilson fermion operator, except with a negative mass parameter $-\rho = 1/2\kappa - 4$ in which $\kappa_c < \kappa < 0.25$. As will explained later in Sec. III, we will use $\kappa = 0.2$ in our calculation which corresponds to $\rho = 1.5$.

The massive overlap Dirac operator is defined so that at the tree-level there is no mass or wave function renormalization [7],

$$D(m) = \rho D_{\mathrm{ov}}(\rho) + m\left(1 - \frac{D_{\mathrm{ov}}(\rho)}{2}\right)$$
$$= \rho + \frac{m}{2} + \left(\rho - \frac{m}{2}\right)\gamma_5 \varepsilon(H_W(\rho)). \qquad (2)$$

Throughout the paper, we shall use the lattice units for dimensionful quantities, except the lattice spacing a will be explicit in figures.

A. Deflation

It has been advocated [14] that using deflation with low eigenmodes can speed up inversion of fermion matrices. It has been applied to the Hermitian system [15,16] to speed up the inner loop inversion of the overlap operator and to non-Hermitian [17] and Hermitian system with multiple right-hand sides [18]. Low-mode deflation has also been applied to domain decomposition [19]. In addition to speeding up inversions, substituting exact low eigenmodes in the noise estimation such as in quark loops [20,21], and all-to-all correlators [22–24] has demonstrated that better results for the meson two- and three-point functions can be obtained with reduced errors.

The massive overlap Dirac operator in Eq. (2) has the same eigenvectors as the massless one, we shall consider the massless Dirac overlap D_{ov}. Because of the normality of D_{ov}, i.e. $D_{\mathrm{ov}}^\dagger D_{\mathrm{ov}} = D_{\mathrm{ov}} D_{\mathrm{ov}}^\dagger$ and the Ginsparg-Wilson relation $\{\gamma_5, D_{\mathrm{ov}}\} = D_{\mathrm{ov}} \gamma_5 D_{\mathrm{ov}}$, the eigenvalues of D_{ov} are on a unit circle with the center at unity. The real and chiral modes are at 0 and 2. Others on the circle are paired with conjugate eigenvalues. In other words, if $|i\rangle$ is an eigenvector of D_{ov}

$$D_{\mathrm{ov}}|i\rangle = \lambda_i |i\rangle, \qquad (3)$$

then $\gamma_5|i\rangle$ is also an eigenvector with eigenvalue λ_i^*,

$$D_{\mathrm{ov}} \gamma_5 |i\rangle = \lambda_i^* \gamma_5 |i\rangle. \qquad (4)$$

To calculate the eigenmodes of D_{ov}, one notes that due to normality and γ_5 Hermiticity $D_{\mathrm{ov}}^\dagger = \gamma_5 D_{\mathrm{ov}} \gamma_5$, γ_5 commutes with $D_{\mathrm{ov}} D_{\mathrm{ov}}^\dagger$, i.e. $[D_{\mathrm{ov}} D_{\mathrm{ov}}^\dagger, \gamma_5] = 0$. Therefore, one can use the Arnoldi algorithm to search for eigenmodes of $D_{\mathrm{ov}} D_{\mathrm{ov}}^\dagger$ with real eigenvalues $|\lambda_i|^2$ which are doubly degenerate with opposite chirality. To obtain the eigenmodes of D_{ov}, one can diagonalize the two chiral modes in D_{ov}. This is much easier than searching in the complex plane for

the eigenmodes of non-normal fermions. Since the nonzero modes are conjugate pairs (Eq. (4)), we need only to save half of them, e.g. those with positive imaginary eigenvalues. When the eigenmodes are calculated, one can proceed with deflation by solving the high-frequency part of the propagator

$$D(m)|X_{L,R}^H\rangle = (1 - P_L)|\eta_{L,R}\rangle, \tag{5}$$

where $P_L = \sum_{i=1}^{n_0+2n_l} |i\rangle\langle i|$ is the projection operator to filter out the low eigenmodes. n_0 is the number of zero modes which are either all left-handed or all right-handed in each configuration. n_l is the number of nonzero low-frequency modes which come in conjugate pairs. In solving Eq. (5), we use the conjugate gradient solver (CGNE) for $D(m)D^\dagger(m)$. In this case, one can utilize the property $D_{\rm ov}D_{\rm ov}^\dagger = D_{\rm ov} + D_{\rm ov}^\dagger$ to save a matrix multiplication in each iteration with the chiral source $|\eta_{L,R}\rangle$ [15,16] and the solution $|X_{L,R}^H\rangle$ has the same chirality as the source. In this case, Eq. (5) can be written as

$$D(m)|X_{L,R}^H\rangle$$
$$= |\eta_{L,R}\rangle - \sum_{i=1}^{n_0+n_l} (|i\rangle\langle i| + \gamma_5|i\rangle\langle i|\gamma_5)|\eta_{L,R}\rangle\left(1 - \frac{1}{2}\delta_{\lambda_i,0}\right)$$
$$= |\eta_{L,R}\rangle - \sum_{i=1}^{n_0+n_l} (1 \mp \gamma_5)|i\rangle\langle i|\eta_{L,R}\rangle\left(1 - \frac{1}{2}\delta_{\lambda_i,0}\right), \tag{6}$$

where the sum is over the zero modes and the low modes on the upper half of the eigenvalue circle. Although we do not calculate it this way, the high-frequency part of the propagator can be written as

$$|X_{L,R}^H\rangle = D^{-1}(m,\rho)|\eta_{L,R}\rangle - \sum_{i=1}^{n_0+n_l}\left[\frac{|i\rangle\langle i|\eta_{L,R}\rangle}{\rho\lambda_i + m(1 - \frac{\lambda_i}{2})}\right.$$
$$\left. + \frac{\mp\gamma_5|i\rangle\langle i|\eta_{L,R}\rangle}{\rho\lambda_i^* + m(1 - \frac{\lambda_i^*}{2})}\right]\left(1 - \frac{1}{2}\delta_{\lambda_i,0}\right). \tag{7}$$

The total high-frequency part of the propagator will be, in the end

$$|X^H\rangle = |X_L^H\rangle + |X_R^H\rangle, \tag{8}$$

given that the source $|\eta\rangle = |\eta_L\rangle + |\eta_R\rangle$.

To accommodate the $SU(3)$ chiral transformation with $\delta\psi = T\gamma_5(1 - 1/2D_{\rm ov})\psi$ [25] which leads to chirally covariant flavor octet quark bilinear currents in the form $\bar\psi\Gamma T(1 - \frac{1}{2}D_{\rm ov})\psi$, it is usually convenient to use the chirally regulated field $\hat\psi = (1 - \frac{1}{2}D_{\rm ov})\psi$ in lieu of ψ in the interpolation field and the currents. This turns out to be equivalent to leaving unchanged the unmodified interpolation field and currents and adopting instead the effective propagator

$$D_{\rm eff}^{-1} \equiv \left(1 - \frac{D_{\rm ov}}{2}\right)D^{-1}(m), \tag{9}$$

which also serves to filter out the unphysical eigenmode at $\lambda = 2\rho$ [26].

Defining $S \equiv D_{\rm eff}^{-1}$ and $S = S_H + S_L$, where S_H/S_L is the high/low-frequency part of the effective propagator, S_H originating from the source η can be obtained, after a few steps of derivation, as

$$\langle x|S_H|\eta\rangle \equiv \sum_y S_H(x,y)\eta(y) = \left\langle x\left|\left(1 - \frac{D_{\rm ov}}{2}\right)\right|X^H\right\rangle$$
$$= \left(1 + \frac{m}{2\rho - m}\right)\langle x|X^H\rangle - \frac{1}{2\rho - m}\langle x|(1 - P_L)|\eta\rangle. \tag{10}$$

It is worthwhile pointing out from Eq. (10) that once $|X^H\rangle$ is solved, there is no need to explicitly multiply $D_{\rm ov}$ on $|X^H\rangle$ which involves an inversion of the kernel H_W^2 in the Zolotarev approximation of the matrix sign function. Similarly, the low-frequency part of S can be obtained from spectral decomposition

$$\langle x|S_L|\eta\rangle \equiv \sum_y S_L(x,y)\eta(y) = \left\langle x\left|\left(1 - \frac{D_{\rm ov}}{2}\right)\right|X^L\right\rangle$$
$$= \sum_{i=1}^{n_0+n_l}\left[\frac{(1 - \frac{\lambda_i}{2})\langle x|i\rangle\langle i|\eta\rangle}{\rho\lambda_i + m(1 - \frac{\lambda_i}{2})}\right.$$
$$\left. + \frac{(1 - \frac{\lambda_i^*}{2})\langle x|\gamma_5|i\rangle\langle i|\gamma_5|\eta\rangle}{\rho\lambda_i^* + m(1 - \frac{\lambda_i^*}{2})}\right]\left(1 - \frac{1}{2}\delta_{\lambda_i,0}\right), \tag{11}$$

Since the eigenmodes are available for the low-frequency modes, one can obtain the all-to-all propagator for this part of the spectrum

$$\tilde S_L(x,y) = \sum_{i=1}^{n_0+n_l}\left[\frac{(1 - \frac{\lambda_i}{2})\langle x|i\rangle\langle i|y\rangle}{\rho\lambda_i + m(1 - \frac{\lambda_i}{2})}\right.$$
$$\left. + \frac{(1 - \frac{\lambda_i^*}{2})\langle x|\gamma_5|i\rangle\langle i|\gamma_5|y\rangle}{\rho\lambda_i^* + m(1 - \frac{\lambda_i^*}{2})}\right]\left(1 - \frac{1}{2}\delta_{\lambda_i,0}\right). \tag{12}$$

In the above expressions, we have suppressed the Dirac and color indices.

B. Low-mode substitution

It is shown [22–24] that when noise is used to estimate the meson two- and three-point correlation functions in the connected insertion, substituting the noise estimated low-mode part of the correlator with the exact one improves statistics. Consider, for example, the meson correlator from the local interpolation fields $O_i = \bar\psi\Gamma_i\psi$ where the two-point correlator is

$$C(t,\vec p;\eta) = \sum_{\vec x,\vec y} e^{-i\vec p\cdot\vec x}\langle\text{Tr}[\Gamma_1 S(\vec x,t;\vec y,0)\eta(\vec y)$$
$$\times \Gamma_2\gamma_5 S^\dagger(\vec x,t;\vec y,0)\eta^\dagger(\vec y)\gamma_5]\rangle, \tag{13}$$

where the source η is on the $t = 0$ time slice with support on $\{\vec y\}$. Since the quark propagator S is composed of the

low-frequency and high-frequency parts $S = S_H + S_L$, the two-point correlation function can be decomposed into the following

$$C = C_{HH} + C_{HL} + C_{LH} + C_{LL}, \qquad (14)$$

where

$$C_{LL} = \sum_{\vec{x},\vec{y},\vec{y}'} e^{-i\vec{p}\cdot\vec{x}} \text{Tr}\langle \Gamma_1 S_L(\vec{x}, t; \vec{y}, 0)\eta(\vec{y})$$

$$\times \Gamma_2 \gamma_5 S_L^\dagger(\vec{x}, t; \vec{y}', 0)\eta^\dagger(\vec{y}')\gamma_5\rangle. \qquad (15)$$

The noise η has the property

$$\langle \eta(\vec{x})\eta^\dagger(\vec{y})\rangle = \delta_{x,y}, \qquad (16)$$

where $\langle\ldots\rangle$ is the noise average. The standard error due to the noise estimation of the correlation function averaged over the gauge configurations is given by [27,28]

$$\epsilon = \sqrt{\frac{\sigma_g^2}{N_g} + \frac{\sigma_n^2}{N_n N_g}}. \qquad (17)$$

where σ_g^2/σ_n^2 is the variance of the gauge/noise ensemble, and N_g/N_n is the number of gauge/noise configurations. How good the approximation is depends on the noise estimation. Through the numerical study of the quark loop for the energy-momentum tensor with the Wilson fermion on quenched gauge configurations, it is learned [28] that σ_n is much larger than σ_g with $\sigma_n/\sigma_g \sim 27(46)$ for the case with (without) 4-term unbiased subtraction. As such, it is desirable to replace the noise estimate of C_{LL} with the exact correlator to reduce variance due to the noise estimation. The low-mode substituted meson correlator is then

$$C(t, \vec{p})_{\text{sub}} = C - C_{LL} + \tilde{C}_{LL}, \qquad (18)$$

with

$$\tilde{C}_{LL} = \sum_{\vec{x},\vec{y}\in G} e^{-i\vec{p}\cdot(\vec{x}-\vec{y})}\text{Tr}\langle \Gamma_1 \tilde{S}_L(\vec{x}, t; \vec{y}, 0)\Gamma_2 \gamma_5 \tilde{S}_L^\dagger(\vec{x}, t; \vec{y}, 0)\gamma_5\rangle,$$

$$\qquad (19)$$

where the sum of $\vec{y}$ runs over the set G with the same support on $\{\vec{y}\}$ as the noise η.

In the case of baryon, one can use the $Z_3 (e^{i2\pi k/3}, k = 0, 1, 2)$ noise on a time slice for the quark source due to the property

$$\langle \eta(\vec{x})\eta(\vec{y})\eta(\vec{z})\rangle_n = \delta_{x,y}\delta_{y,z}, \qquad (20)$$

so that it is an approximation for the superposition of multiple baryon source with three quarks in each of the baryon originating from the same spatial location on the support of the Z_3 noise.

Similar to the meson case, one can substitute C_{LLL}, which is the part with all three quarks estimated by $S_L\eta$, with $\tilde{C}_{LLL}$ where all three quark propagators are given in terms of $\tilde{S}_L$. In addition, one can replace the C_{HLL} part,

where one of the quark propagators is $S_H\eta$ and the other two are $S_L\eta$, by $\tilde{C}_{HLL}$ in which the product of the two $S_L\eta$ is replaced by $\sum_{\vec{y}} S_L(\vec{x}, t; \vec{y}, 0)S_L(\vec{x}', t; \vec{y}, 0)\eta^\dagger(\vec{y})$.

$$C(t, \vec{p})_{\text{sub}} = C - C_{LLL} + \tilde{C}_{LLL} - P\{C_{HLL}\} + P\{\tilde{C}_{HLL}\}$$

$$\qquad (21)$$

where $P\{\}$ refers to the set of correlators with permutation of $S_H\eta$ and $S_L\eta$ (or $\tilde{S}_L$) for the three different quarks in the baryon. It is worthwhile pointing out that $\tilde{C}_{HLL}$ is like C_{HL} in the meson in the sense that the error due the noise is from σ_n associated with Eq. (16). To the extent that the baryon correlator is dominated by C_{LLL} and $P\{C_{HLL}\}$ in the time window where the ground state baryon emerges, the variance reduction with the substitution in Eq. (21) is expected to be similar to that of the meson case.

III. NUMERICAL DETAILS

The overlap propagators are calculated on three sets of lattices of the $2 + 1$ flavor domain-wall fermion gauge configurations with the four-dimensional sizes of $16^3 \times 32$, $24^3 \times 64$ ($a^{-1} = 1.73(3)$ GeV), and $32^3 \times 64$ ($a^{-1} = 2.32(3)$ GeV) with several sea quark masses each. These are generated by the RIKEN-Brookhaven-Columbia (RBC) collaboration and the UKQCD collaboration [1–3]. The matrix sign function in the overlap Dirac operator is calculated with 14th degree Zolotarev rational polynomial approximation [7,29]. For the window [0.031, 2.5], the approximation to the sign function is better than 3.3×10^{-10} [7]. This is sufficiently accurate as the low-mode deflation is used in the inversion of H_W with HYP smearing in the Zolotarev approximation, which is the inner loop of the inversion of the overlap operator, and the largest absolute values of the low-mode eigenvalues are 0.2, 0.125, and 0.22 on $16^3 \times 32$, $24^3 \times 64$, and $32^3 \times 64$ lattices with 100, 400, and 200 eigenvectors, respectively. As shown in Figs. 1(a), 2(a), and 3(a), the largest absolute values of the projected eigenvalues on the HYP smeared configurations are larger than 0.031, the threshold for high accuracy of the approximation of the sign function.

A. Speedup of propagator calculation

We employ HYP smearing [30] on the gauge links which has the effect of depleting the density of the lowest eigenvalues in H_W [31]. As a result, the lowest eigenvalue with HYP smearing after deflation with 100 to 200 eigenmodes is about 3 times larger than those without HYP smearing. This leads to $\sim$3 times speedup in the number of inner loop conjugate gradient (CG) iterations as was found in a previous study [31]. This is tabulated in Table I. In addition, for the three lattices under study, the numbers of H_W/D_{ov} eigenmodes used for deflation in the inner/ outer loop, the numbers of inner and outer iterations for the cases without deflation, with deflation, and with both deflation and HYP smearing. For the comparison study, we
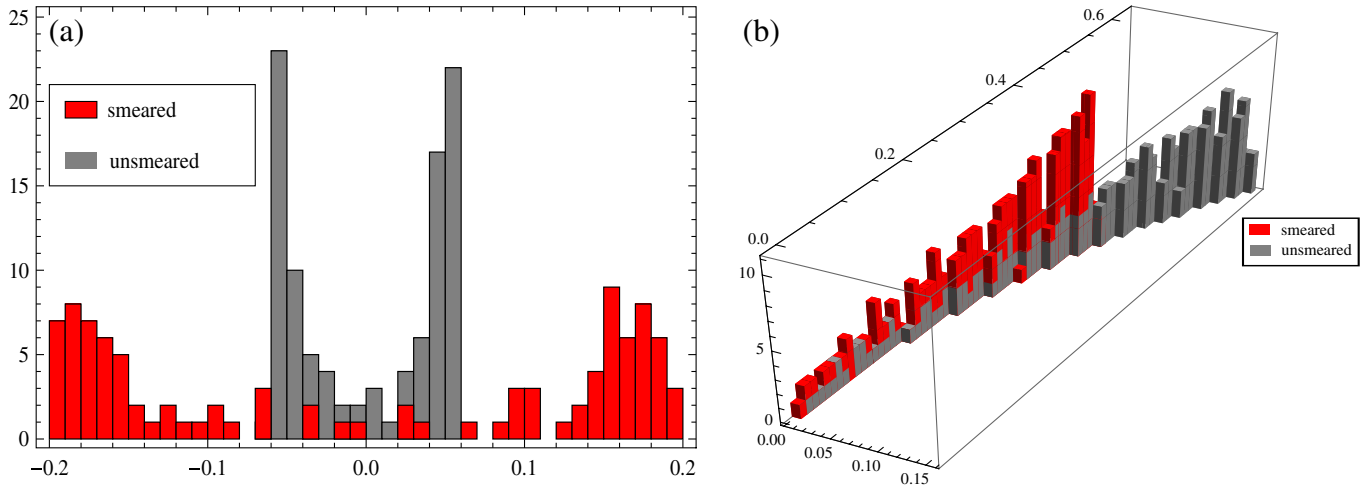
FIG. 1 (color online). (color online) (a) The spectra of the lowest 100 eigenvalues for the kernel in the inner loop of the overlap fermion for a $16^3 \times 32$ configuration with $m_l = 0.01$. (b) The same as (a) for the lowest 200 eigenvalues of the outer loop overlap fermion. The unsmeared spectra are colored in grey and the HYP smeared spectra are colored in red.

used light sea mass at $m_l = 0.01$, 0.005 and 0.004 for the $16^3 \times 32$(lattice16), $24^3 \times 64$(lattice24) and $32^3 \times 64$(lattice32) lattices which are, respectively, the lowest light sea mass in these three lattice sets. For the valence quark, we used the quark mass which corresponds to the pion mass at ~ 200 MeV in all three cases. We see from Table I that the inner loop iteration number is reduced by a factor of ~ 3 due to HYP smearing. One can see from Figs. 1(a), 2(a), and 3(a), that this is due to the fact that after projecting out the small eigenvalues of H_W^2, the resultant lowest eigenvalue with smearing is about a factor of 3 larger than those without smearing. On the other hand, the number of outer iterations are greatly reduced due to deflation of the low $D_{\rm ov}$ eigenmodes. It is interesting to note that the number of outer iteration for deflation with the

smearing case is $\sim 18\%$–25% higher than the corresponding case without smearing. This is due to the fact that after HYP smearing, the imaginary parts of the highest eigenvalues of the deflated eigenmode $\lambda_{\rm max}$ at $0.0707 \pm i0.434$ (lattice 16), $0.00857 \pm i0.153$ (lattice 24) and $0.0115 \pm i0.186$ (lattice 32) are 46%, 51%, and 22% smaller than those of the corresponding eigenvalues without smearing. This can be seen in Figs. 1(b), 2(b), and 3(b). In the end, when the total number of iterations are compared, the speedup with deflation and smearing to the cases without them are 23, 51, and 79 times, respectively, for the three lattices for one test configuration each. The three selected configurations have zero modes. We have also tested configurations without zero modes. It turns out the total numbers of iterations for both the cases with and without
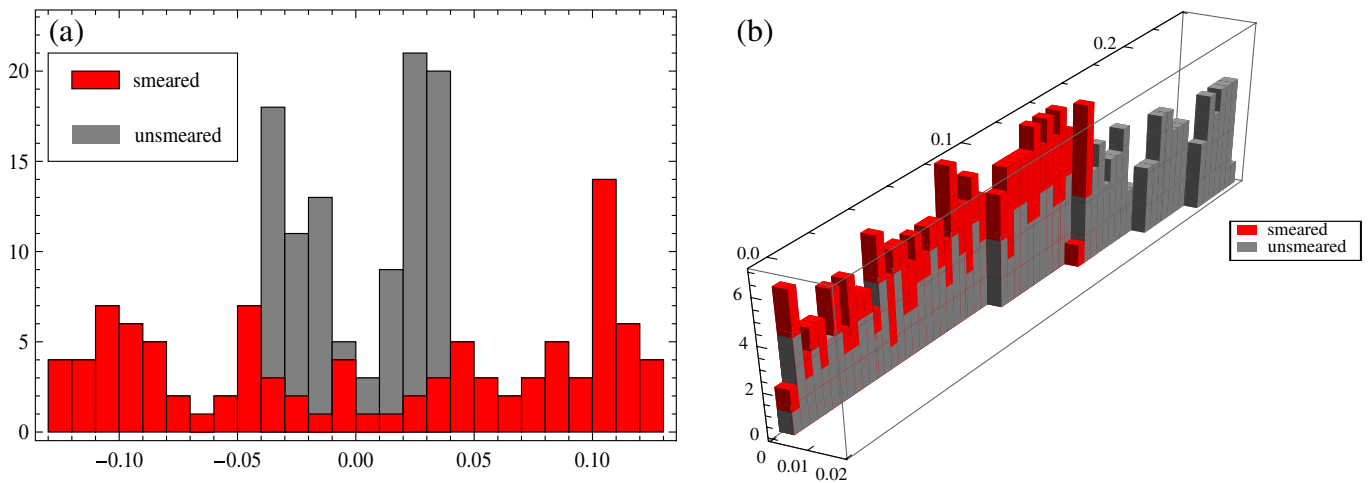

FIG. 2 (color online). (color online) (a) The spectra of the lowest 400 eigenvalues for the kernel in the inner loop of the overlap fermion for a $24^3 \times 64$ configuration with $m_l = 0.005$. (b) The same as (a) for the lowest 200 eigenvalues of the outer loop overlap fermion. The unsmeared spectra are colored in grey and the HYP smeared spectra are colored in red.
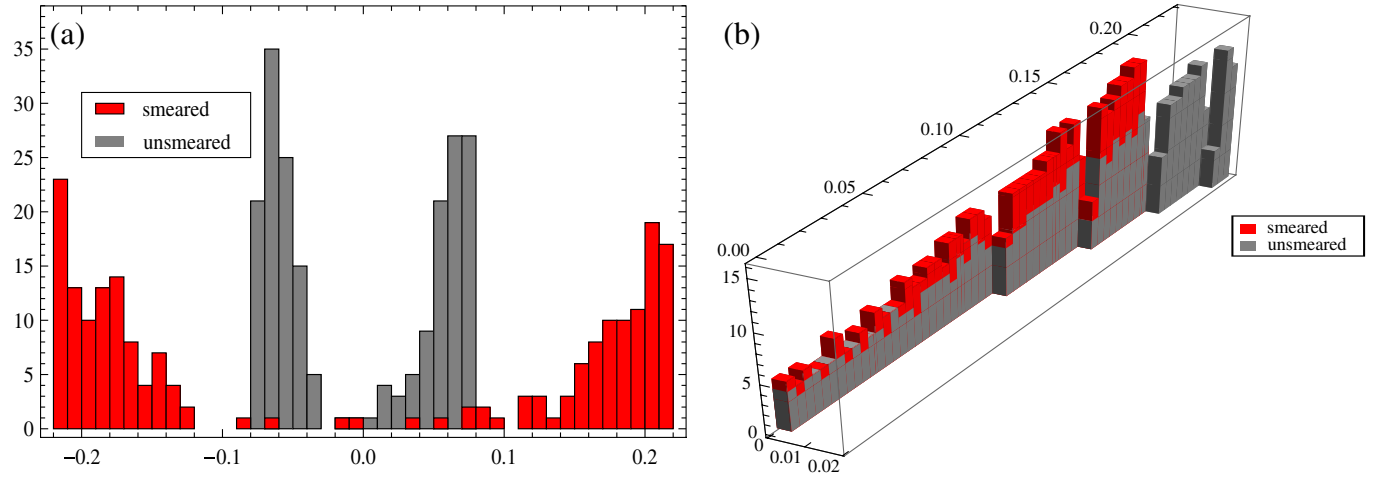
FIG. 3 (color online).   (color online) (a) The spectra of the lowest 200 eigenvalues for kernel in the inner loop of the overlap fermion for a $32^3 \times 64$ configuration with $m_l = 0.004$. (b) The same as (a) for the lowest 400 eigenvalues of the outer loop overlap fermion. The unsmeared spectra are colored in grey and the HYP smeared spectra are colored in red.

smearing and deflation are about the same as those of configurations with zero modes. This is so because the absolute eigenvalues of the lowest eigenmodes for configurations without zero modes (which are of the order 10^{-2} for the $16^3 \times 32$ lattice, 10^{-3} for the $24^3 \times 64$ lattice, and 10^{-4} for the $32^3 \times 64$ lattice) are comparable to the smallest quark masses on these lattices.

We should point out that the absolute values of the above-mentioned $\lambda_{\max}$ of the low-frequency modes on these lattices are much larger than the small valence quark masses (ranging from 0.0014 to 0.01, for instance) so that the small valence quark does not affect the speed of inversion and, thus, there is no critical slowing down for the light valence masses in inversions with low-mode deflation. Also listed is the overhead for producing eigenmodes of the overlap fermion for deflation. The cost is in the range of 4.5 to 7.9 propagators with both deflation and HYP smearing $(D + S)$. This cost is to be amortized when more propagators are needed in calculations such as three-point functions and quark loops. To compare with inversion of the Wilson-type fermion, we timed the inversion of the clover

fermion on 10 $2 + 1$ flavor dynamical clover configurations with a size of $32^3 \times 64$ and pion mass of 156 MeV at lattice spacing $a = 0.09$ fm from the PACS-CS Collaboration [32]. Using the CG solver with odd/even preconditioning and no HYP smearing, we find the average inversion of one propagator with the same residual of 10^{-8} takes ~11892 iterations. Taking the product of the inner and outer loop iterations for the case of lattice 32 in Table I, the overlap inversion with smearing and deflation has about 32% more iterations than that of the clover fermion in this case.

B. Tuning of ρ

We carry out the valence quark propagator calculation with 30 quark masses which cover the range from the physical pion mass to the charm mass. There will be a concern about the large finite volume effect for the pion mass as low as the physical one, we shall use those below $m_\pi = 200$ MeV for the finite volume study not in chiral extrapolation. To include the charm mass entails making sure that the heavy mass will have small enough $O(m^2 a^2)$ error to warrant reliable calculation for the charmonium

TABLE I.   Speedup comparison of inversion with HYP smearing (S) and deflation (D) of the outer loop. The inner and outer iteration numbers are the average of one column in one propagator with 12 columns of color-spin. The speedup refers to that between the case of $D + S$ vs the one with neither D nor S. The overhead of producing eigenmodes is measured in terms of the propagators with $D + S$ calculation.

$16^3 \times 32$					$24^3 \times 64$			$32^3 \times 64$		
	residual	w/o D	D	D + S	w/o D	D	D + S	w/o D	D	D + S
H_W eigenmodes	10^{-14}	100	100	100	400	400	400	200	200	200
D_{ov} eigenmodes	10^{-8}	0	200	200	0	200	200	0	400	400
Inner iteration	10^{-11}	340	321	108	344	341	107	309	281	101
Outer iteration	10^{-8}	627	72	85	2931	147	184	4028	132	156
Speedup				23			51			79
Overhead			4.5 propagators			4.9 propagators			7.9 propagators	

and charm-light mesons. To this end, we fine-tune the negative mass parameter ρ in Eq. (2) in the range $1 < \rho < 2$ to minimize the $O(m^2 a^2)$ error. We conducted a test on ten $16^3 \times 32$ ($m_l = 0.01$) configurations for the range of $1.059 < \rho < 1.917$ to check the speed of inversion and $O(m^2 a^2)$ error assessed with the hyperfine splitting (the difference between the vector and pseudoscalar meson masses). It turns out that $\rho = 1.5$ is close to the optimal choice. It has about the fastest inversion and its $m^2 a^2$ error as measured by the hyperfine splitting in the charmonium is the smallest. To illustrate what one means to have the smallest $O(m^2 a^2)$ error, we plot the hyperfine splitting as a function of ma for the case of $\rho = 1.5$ and 1.62 in Figs. 4 and 5 for comparison. The hyperfine splittings for $\rho = 1.5$ and 1.62 are plotted in Figs. 4(a) and 5(a) as a function of m. In view of the fact that the excitation scales for the charmonium and the upsilon as measured from the $2S$ to $1S$ and the average 1^3P to 1^3S splittings are about the same, it is argued [33] based on nonrelativistic Schrödinger

equation that the size of the heavy quarkonium should scale as

$$r_{Q\bar{Q}} \propto \frac{1}{\sqrt{m}}. \tag{22}$$

This prediction is checked against the leptonic decay widths, the fine and hyperfine splittings [33] of charmonium and upsilon. In the case of the hyperfine splitting, the perturbative spin-spin interaction has the form $\frac{4\pi\alpha_s}{9} \times \frac{\sigma_1 \cdot \sigma_2}{m_1 m_2} |\Psi(0)|^2$, where $\Psi(0)$ is the vector meson wave function at the origin which is proportional to $r_{Q\bar{Q}}^{-3/2}$. Thus, the hyperfine splitting of the heavy quarkonium is expected to scale like

$$\Delta E_{\text{HFS}} \propto \frac{1}{\sqrt{m}} \tag{23}$$

to leading order in m. Based on this observation, we plot the hyperfine splitting (HFS) for $\rho = 1.5$ and 1.62 in

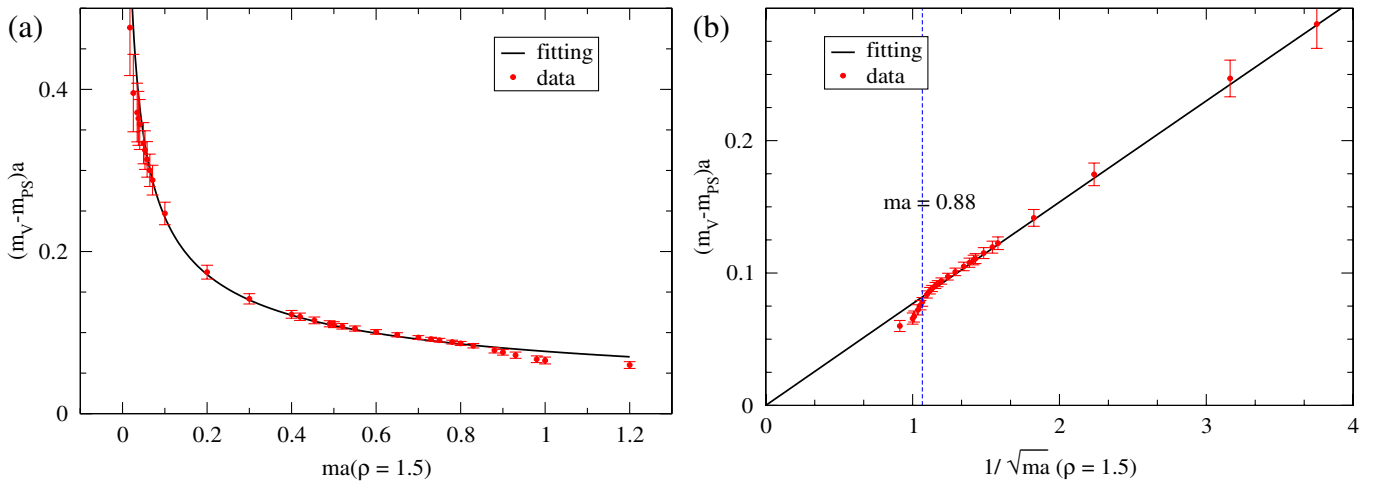FIG. 4 (color online).   The hyperfine splitting is plotted as a function of ma in (a) and $1/\sqrt{ma}$ in (b). This is for $\rho = 1.5$.
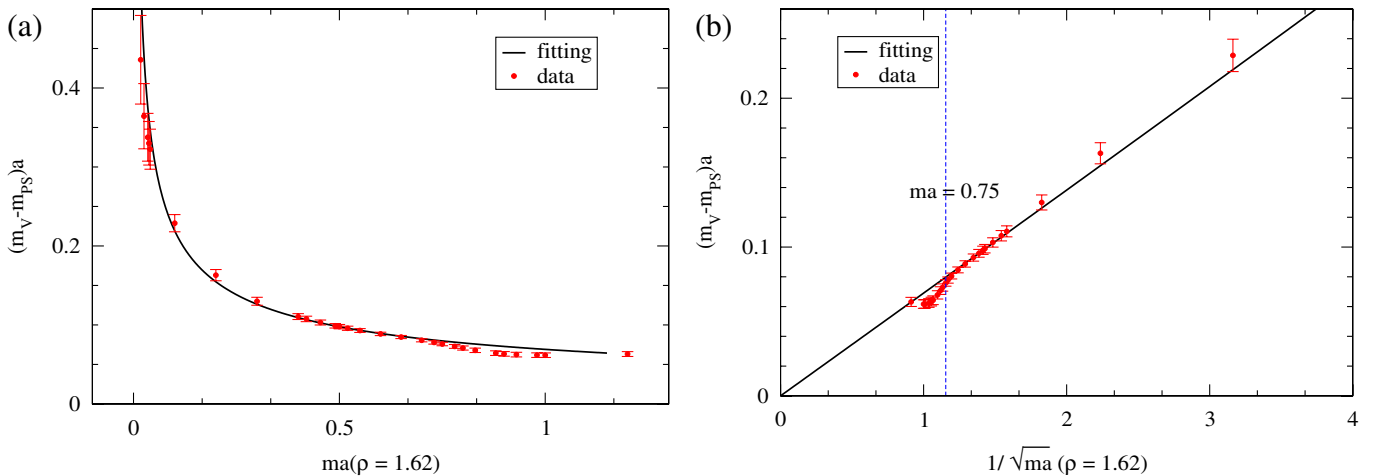

FIG. 5 (color online).   The hyperfine splitting is plotted as a function of ma in (a) and $1/\sqrt{ma}$ in (b). This is for $\rho = 1.62$.

Figs. 4(b) and 5(b) in terms of $1/\sqrt{m}$. We see that in both cases, the HFS trends toward zero as m is heavier than 0.4, except for a few points at the heavy end which show large deviation from the trend. We interpret this as due to the lattice $O(m^2 a^2)$ error. To find a threshold of usable range of m where the estimated $O(m^2 a^2)$ error is negligible (or smaller than the statistical error), we fit the HFS to the form

$$\Delta E_{\text{HFS}} = \frac{a}{\sqrt{m}}\left(1 + \frac{b}{m}\right), \qquad (24)$$

which includes the next term in large m expansion. From the fit in the range $m = 0.4/0.6$ to 0.8 for $\rho = 1.5/1.62$ (which corresponds to $1/\sqrt{m} = 1.58/1.29$ to 1.12), we find $a = 0.0769(6)/0.0690(7)$ and $b = -0.0002(19)/0.0004(29)$ for $\rho = 1.5/1.62$. We see that the central value of b/m is much smaller than its error and is thus consistent with zero in both cases. At the heavy-mass end, the central values of the HFS are outside the fits. We find that at $m = 0.88/0.75$ for $\rho = 1.5/1.62$, the central value is beginning to be more than 2σ away from the fitted HFS curve. We take it to be the critical value beyond which there is discernible $O(m^2 a^2)$ error. This suggests that, given the same relative deviation, $\rho = 1.5$ has a longer range of usable m than $\rho = 1.62$. Thus, we decide to adopt $\rho = 1.5$. In this case, the charm quark is at ~ 0.73 where the central value of the HFS is consistent with the fitted curve well within one sigma (relative error is about 1%). Through study of the $O(m^2 a^2)$ error with different lattice spacings for the overlap fermion, it is found [34] that the critical mass is insensitive to the lattice spacing and depends mostly on ma. For the $32^3 \times 64$ lattice at $a^{-1} = 2.32$ GeV, the charm mass is at $m \sim 0.48$, which is much smaller than the critical mass $ma = 0.88$.

We conclude that we can cover the quark mass range from light all the way to the charm with the overlap fermion on the three sets of DWF configurations under study. The critical mass of $ma \sim 0.88$ for a discernible $O(m^2 a^2)$ error in the HFS is higher than that of the quenched case where the $O(m^2 a^2)$ error becomes appreciable (5%) when $ma \sim 0.5$ [26]. This is presumably due to HYP smearing that is adopted in the present calculation with dynamical fermion configurations. HYP smearing is also known to improve the locality of the overlap operator [31,35].

C. Zero mode issue

The role of zero modes and topology at finite volume has been discussed extensively in the literature [36]. The cal-culation of the quark condensate $\langle \bar{\psi}\psi \rangle$ with the chiral fermion contains a term from the zero mode contribution $\frac{\langle |Q| \rangle}{mV}$ where Q is the topological charge of the configuration which, according to Atiya-Singer theorem, equals the difference between the numbers of left-handed and right-handed zero modes. This term vanishes in the limit $V \to \infty$ ($\langle |Q| \rangle$ grows as $\sqrt{V}$) for finite m. It is shown [36] that as long as one is working in the region where $m\Sigma V \gg 1$, the

zero mode contribution to the quark condensate is negli-gible as the number of zero modes per unit volume goes to zero when the volume approaches infinity. Based on this and the generalized Gell-Mann-Oakes-Renner relation

$$\frac{1}{V}\int d^4x d^4y \langle \pi^a(x)^\dagger \pi^a(y) \rangle = -\frac{2}{m}\langle \bar{\psi}\psi \rangle, \qquad (25)$$

where $\pi^a = \bar{\psi}\gamma_5 \tau^a/2\psi$, it is suggested [37,38] that, as long as $m\Sigma V \gg 1$, the contribution of the zeros to the pseudoscalar correlator is negligible. In this case, one expects to obtain the pseudoscalar mass from the exponen-tial fall off of the correlator. To test this idea, we plot in Fig. 6 the correlators for the pseudoscalar masses at ~ 200, 350, 700 and 2980 MeV. on the $16^3 \times 32$ lattice for one gauge configuration with and without zero mode contribu-tions (there are two zero modes in this configuration) for the purpose of illustration. We see that when the pion mass is as low as 200 MeV, where $m\Sigma V \sim 1.8$ is not much larger than unity, the pion correlator is greatly affected. The pion mass may not change very much, but the spectral weight is reduced by an order of magnitude when the zero modes are taken out. When the pion mass is $\sim 350/700$ MeV where $m\Sigma V \sim 5.5/22$, we see that the correlators are not affected much when the zero modes are taken out. This seems to conform with the above idea. However, when we plot the correlator without the zero modes and examine the heavy quark case where $m\Sigma V \gg 1$ is satisfied, we see that the correlators with and without the zero modes differ by several orders of magnitude at large time separation, e.g. $t > 10$. This is so because the zero mode contribution normalized in the present volume is of the order $> 10^{-8}$ at large time separation; whereas, the signal for the pseu-doscalar meson falls off exponentially with respect to time.
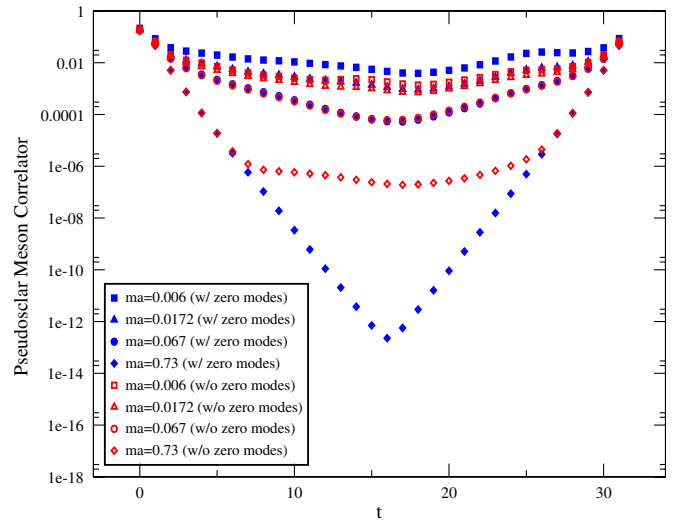

FIG. 6 (color online). (color online) The pseudoscalar meson correlators for pion masses at ~ 200, 350, 700 and 2980 MeV which correspond to the input quark masses at 0.006, 0.0172, 0.067, and 0.73 for a configuration of the $16^3 \times 32$ lattice with and without zero mode contributions.

Sooner or later, the signal will fall below the zero mode contribution. In other words, the zero mode at any finite volume is part of the physical spectrum. Except for quark condensate and other rare cases, one cannot separate out the zero mode contribution from the rest of the spectrum for physical observables in general. Even though it may not make much of a difference numerically for the meson correlator at relatively short range of t when $m\Sigma V \gg 1$, the large time separation will sooner or later be affected and this problem is more acute for the heavy quark.

IV. RESULTS

Since the overlap fermion is calculated on configurations generated with domain-wall fermions, this constitutes a mixed-action approach to chiral fermions. Mixed-action approaches have been studied by several groups, such as DWF valence on staggered fermion sea [9], overlap valence on DWF sea [10], overlap valence on clover sea [11], and overlap valence on twisted fermion sea [12]. In view of the fact that it is numerically intensive to simulate chiral fermions (DWF or overlap), it is practical to use the cheaper fermion formulation for generating gauge configurations and the chiral fermion for the valence as an expedient approach toward full unquenched QCD simulation with chiral fermions. Many current algebra relations depend only on the chiral property of the valence sector. The mixed-action theory with different fermions for the valence and the sea is a generalization of the partially quenched theory with different sea and valence quark masses. The mixed-action partially quenched chiral perturbation theory (MAPQχPT) has been developed for Ginsparg-Wilson fermion on Wilson sea [39] and staggered sea [40], and has been worked out for many hadronic quantities to next-to-leading order (NLO), such as pseudoscalar masses and decay constants [39–41], isovector scalar a_0 correlator [42–45], heavy-light decay constants [46], and baryon masses [45,47].

In the mixed-action chiral perturbation theory with chiral valence fermion, it is shown [39] that to NLO, there is no $\mathcal{O}(a^2)$ correction to the valence-valence meson mass due to the chiral symmetry of the valence fermion. Furthermore, both the chiral Lagrangian and the chiral extrapolation formulas for hadron properties to the one-loop level (except θ-dependent quantities) are independent of the sea fermion formulation [48]. The LO mixed-action chiral Lagrangian invokes only one more term with $\mathcal{O}(a^2)$ discretization dependence which is characterized by a low-energy constant Δ_{mix}. The LO pseudoscalar meson masses are given as

$$m_{vv'}^2 = B_{\mathrm{ov}}(m_v + m_{v'}),$$
$$m_{vs}^2 = B_{\mathrm{ov}}m_v + B_{dw}(m_s + m_{\mathrm{res}}) + a^2\Delta_{\mathrm{mix}}, \qquad (26)$$
$$m_{ss'}^2 = B_{dw}(m_s + m_{s'} + 2m_{\mathrm{res}}),$$

where $m_{vv'}/m_{ss'}$ is the mass of the pseudoscalar meson made up of valence/sea quark and antiquark. m_{vs} is the mass of the mixed valence and sea pseudoscalar meson. Up to numerical accuracy, there is no residual mass for the valence overlap fermion. The DWF sea has a residual mass m_{res} which vanishes as $L_S \to \infty$. The Δ_{mix} enters in the mixed meson mass m_{vs} and is an $\mathcal{O}(a^2)$ error which vanishes at the continuum limit. We should note that, unlike the partially quenched case, even when the quark masses in the valence and sea match, the unitarity is still violated due to the mixed-action. The degree of unitarity violation at finite lattice spacing depends on the size of Δ_{mix}.

A. Calculation of Δ_{mix}

Δ_{mix} has been calculated for pseudoscalar mesons for DWF valence and staggered fermion sea [44,49] which gives $\Delta_{\mathrm{mix}} \sim (708 \text{ MeV})^4$ [49] and $\sim(664 \text{ MeV})^4 \pm (437 \text{ MeV})^4$ [44]. It is also calculated for overlap valence and clover sea which yields $\Delta_{\mathrm{mix}} = (872 \text{ MeV})^4 \pm (693 \text{ MeV})^4$ [50]. This means that for a valence pion of 300 MeV, the Δ_{mix} produces, at $a = 0.12$ fm, a shift of ~ 102–251 MeV for these cases, which is quite large.

Here we shall estimate Δ_{mix} in our case with overlap valence on DWF sea. To do so, we shall examine the meson state which wraps around the time boundary. It is known that a two-meson interpolation field can produce meson states with two mesons propagating along opposite-time directions [51–53]. On the other hand, the a_0 isovector scalar meson interpolation field $\bar{u}d$, together with the quark loop from the sea, can produce a π and $\eta(\eta')$ propagating in different time direction [54]. This is illustrated in Fig. 7 where Fig. 7(a) displays the situation with both the valence and the sea quarks wrapping around the time boundary forming two pions propagating in different time directions;
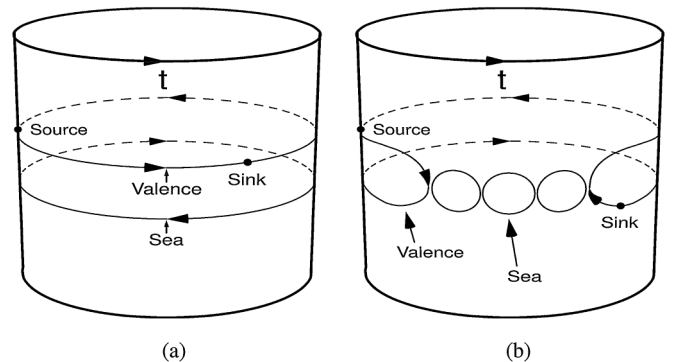
FIG. 7. Cartoon showing the quark lines which form wrap-around π and η mesons in the a_0 correlator. (a) Both the valence and the sea wrap around the time direction and form two pions which are propagating in different time directions. (b) The annihilation diagram where only the valence wraps around the time boundary. Together with (a), it produces π and $\eta(\eta')$ propagating in different time directions.

whereas, Fig. 7(b) shows the annihilation diagram where the valence quark-antiquark pair wraps around the time boundary while the sea quark loops do not. Together, Fig. 7(a) and 7(b) form an opposite-time propagating π and $\eta(\eta')$ pair. The a_0 correlator has, thus, the following form

$$
\begin{aligned}
C_{a_0} &= \sum_i W_i (e^{-E_i t} + e^{-E_i(T-t)}) + W_{\pi\eta}(e^{-m_\pi t - m_\eta(T-t)} \\
&\quad + e^{-m_\eta t - m_\pi(T-t)}), \\
&= \sum_i 2W_i e^{-E_i T/2} \cosh(E_i(T/2 - t)) \\
&\quad + 2W_{\pi\eta} e^{-(m_\pi + m_\eta)T/2} \cosh((m_\eta - m_\pi)(T/2 - t)),
\end{aligned}
\tag{27}
$$

where E_i is the energy of one- or two-meson state which propagates in the same time direction. Notice that the second term in Eq. (27), which represents the η and π wrapping around the time boundary, has an exponential falloff which is proportional to the mass difference of η and π, i.e., $m_\eta - m_\pi$. Since this is smaller than all the other states in the a_0 correlator,[1] it appears as the lowest state in the longest time separation in the correlator. This low-lying state causes problems for fitting the scalar correlator to obtain the a_0 meson [54].

We shall take advantage of the existence of this state due to the finite time extent to extract Δ_{mix}. As we see in Fig. 7, the structure of Fig. 7(b) is complicated. Yet, Fig. 7(a) is simple in that it involves the mass difference of two pions, not η and π as in Eq. (27). For the equal valence quark mass case, the mass difference of the two pions vanishes and one does not obtain any information about Δ_{mix}. But if the two valence quark masses are not the same, the mass difference of the two pions becomes

$$
\begin{aligned}
m_{v_1 s} - m_{v_2 s} &= \sqrt{B_{\text{ov}} m_{v_1} + B_{dw}(m_s + m_{\text{res}}) + a^2 \Delta_{\text{mix}}} \\
&\quad - \sqrt{B_{\text{ov}} m_{v_2} + B_{dw}(m_s + m_{\text{res}}) + a^2 \Delta_{\text{mix}}},
\end{aligned}
\tag{28}
$$

where $m_{v_1 s}/m_{v_2 s}$ is the pion made of quarks with v_1/v_2 overlap fermion and the s domain-wall fermion. In this case, one can extract Δ_{mix}. To do so, one needs to remove the annihilation diagram in Fig. 7(b) and all the states which propagate in the same time direction. This can be achieved by calculating the valence propagators with both antiperiodic and periodic boundary conditions in time (the DWF sea has antiperiodic B.C.), and taking the difference of the two correlators. For the annihilation diagram in

---

[1] We should note that there are states where π and η move back to back with nonzero momenta which have smaller energy differences, but they will be suppressed by the corresponding prefactor $e^{-(E_\pi + E_\eta)T/2}$ as compared to $e^{-(m_\pi + m_\eta)T/2}$ in Eq. (27) for the the zero-momentum $\pi - \eta$ state for large T.

Fig. 7(b), the valence quark traverses the time boundary an even number of times so that it is independent of the time boundary condition. On the contrary, the valence quark in Fig. 7(a) traverses the time boundary an odd number of times. So, taking the difference between correlators with periodic and antiperiodic time B.C. for the valence cancels out the annihilation diagram in Fig. 7(b) as well as the contribution from states propagating in the same time direction, and one is left with the contribution in Fig. 7(a).

As a first attempt to extract Δ_{mix}, we consider the difference of scalar correlators from the $24^3 \times 64$ DWF lattice (light sea mass at $m_l = 0.005$) with periodic and antiperiodic B.C. in time. In this case, the difference correlator at large time will be given by

$$
\begin{aligned}
\Delta C_{a0} = C_{a_0}^P - C_{a_0}^{AP} &\rightarrow 4W_{\pi_1\pi_2} e^{-(m_{v_1 s} + m_{v_2 s})T/2} \\
&\times \cosh\{(m_{v_1 s} - m_{v_2 s})(T/2 - t)\}.
\end{aligned}
\tag{29}
$$

As a first check, we plot, in Fig. 8, such a difference correlator for the equal valence case (i.e. $m_{v_1} = m_{v_2}$). We expect, from Eq. (29), that the correlator should be independent of t. As we see in Fig. 8, where such correlators are plotted for $m_{v_1} = m_{v_2} = 0.0203$ and 0.0489, which correspond to pion masses at ~ 372 and 577 MeV, the correlators are indeed quite flat. This is consistent with our expectation that the large t behavior depends on the mass difference $m_{v_1 s} - m_{v_2 s}$ which is zero in this case. To extract Δ_{mix}, we want to find a range of quark mass where the tree-level linear mass relation between m_{vv}^2 and m_v holds so that we can use Eq. (26). We plot m_{vv}^2 and m_{vv}^2/m_v from the $24^3 \times 64$ lattice with $m_l = 0.005$ as a function of m_v in Fig. 9.

We see that the ratio $m_{vv}^2 a^2/m_v a$ in Fig. 9(b) is fairly flat for the range $m_v a \sim 0.0203$–0.0489. We shall take m_{v_1} and
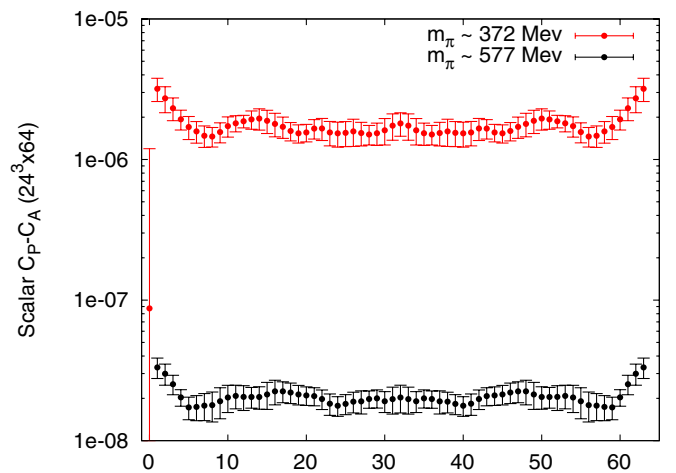

FIG. 8 (color online). The difference of the scalar (a_0) correlators with antiperiodic and periodic time boundary conditions for the two equal valence masses which correspond to $m_\pi = 372$ and 577 MeV.
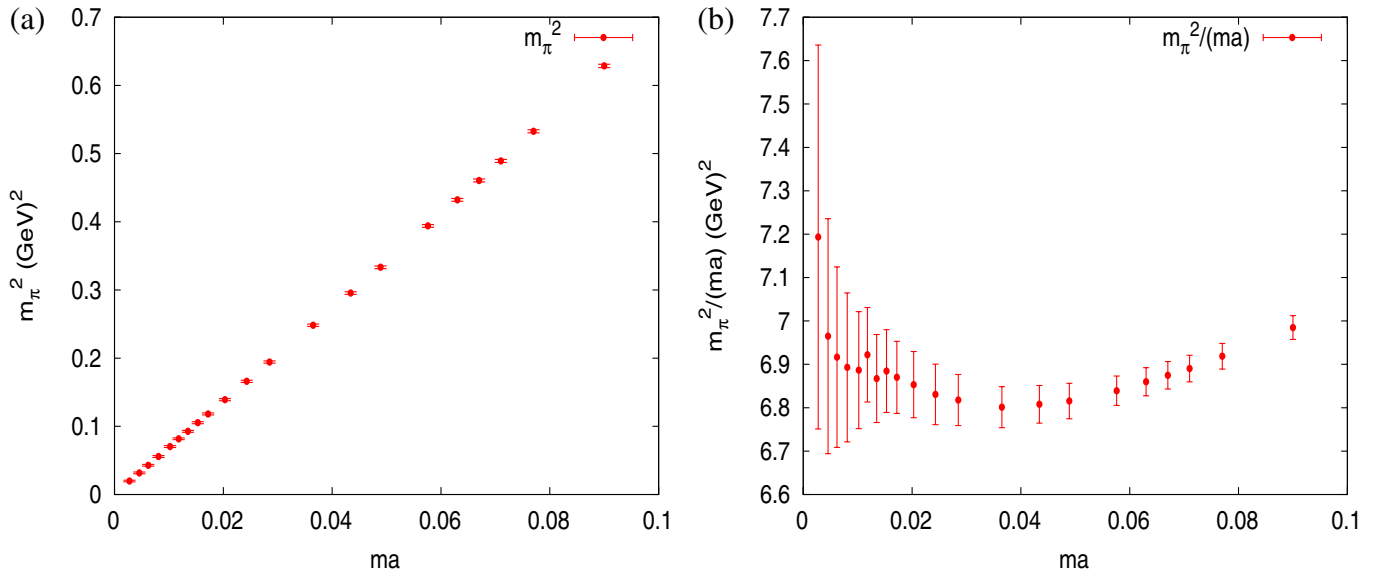
FIG. 9 (color online). (a) m_π^2 in GeV^2 is plotted as a function of ma for the $24^3 \times 64$ lattice with $m = [0.00275, 0.15]$. (b) m_π^2/ma in GeV^2 is plotted vs ma for the same range of quark masses.

m_{v_2} from this range and fit the correlators to find $m_{v_1s} - m_{v_2s}$ which can be expressed in terms of the corresponding pseudoscalar masses and Δ_{mix},

$$m_{v_1s} - m_{v_2s} = \sqrt{\frac{1}{2}(m_{v_1v_1}^2 + m_{ss}^2) + a^2\Delta_{\text{mix}}}$$
$$- \sqrt{\frac{1}{2}(m_{v_2v_2}^2 + m_{ss}^2) + a^2\Delta_{\text{mix}}}. \quad (30)$$

From the separately calculated $m_{v_1v_1}$ and $m_{v_2v_2}$ with the valence overlap fermion and m_{ss} calculated with DWF [2], we can extract Δ_{mix}.

Since the range of $m_v a \sim 0.0203$–0.0489 is narrow, and $m_{v_1v_1}$ and $m_{v_2v_2}$ are close, the errors on the extracted Δ_{mix} from Eq. (30) are large. We take several combinations of $m_{v_1v_1}$ and $m_{v_2v_2}$ in the range [0.0203, 0.0489] and obtain an average Δ_{mix}

$$a^2\Delta_{\text{mix}} = -0.0112(44) \text{ GeV}^2, \quad (31)$$

for the $24^3 \times 64$ lattice with 50 configurations at $m_l = 0.005$. With $a^{-1} = 1.73$ GeV, we obtain

$$\Delta_{\text{mix}} = -(427 \text{ MeV})^4 \pm (338 \text{ MeV})^4. \quad (32)$$

This is quite small. To compare with those from other mixed actions, we notice that the central value is ~ 7 times smaller than the case of DWF valence on staggered sea [44,49] and ~ 18 times smaller than that of overlap on Wilson sea [11]. To put the magnitude in perspective, consider a 300 MeV pion on the $24^3 \times 64/32^3 \times 64$ lattice with $a \sim 0.12/0.085$ fm, the shift in mass due to Δ_{mix} is $\sim 19/10$ MeV which is substantially smaller than the ~ 102–251 MeV for the other mixed actions as alluded to earlier. As mentioned above, the calculation of Δ_{mix} using

the boundary condition method gives large errors. At this stage, we are more interested in finding out how large Δ_{mix} is, roughly to see if it is practically small enough to carry out chiral extrapolation with MAPQχPT. For a more precise value, we shall use the mixed valence DWF and overlap propagators to directly evaluate Δ_{mix} and check scaling as is done in Refs. [11,44,49].

Coming back to the correlators in Fig. 8, we notice that the magnitudes of these two correlators differ by 2 orders of magnitude, a feature which is unusual for meson correlators with pion masses which are not that different. In this case, we note that there is a prefactor $e^{-(m_{v_1s}+m_{v_2s})T/2}$ in Eq. (29) which can be sensitive to slightly different pion mass when T is large. Since we expect the ratio of the spectral weight $W_{\pi_1\pi_2}$ in Eq. (29) for the two correlators with pion masses at ~ 372 and 577 MeV to be within $\sim 20\%$ from unity when the mass dependence of the matrix element and the normalization factor are taken into account, the primary difference of the correlators in Fig. 8 for the equal masses case should come from the exponential prefactor. Taking Δ_{mix} into account, the ratio of the prefactor is 88(13) with $T = 64$. This turns out to be quite close to the jackknife ratio of the calculated correlators in the time range [12,54] which is 83(9). This lends further support for the existence of the wraparound states.

B. Z_3 grid source and low-mode substitution

Noise has been used to estimate quark loops as well as propagators in the all-to-all correlators. In particular, Z_2 noise has been introduced to estimate the quark loops [55] and it is shown [55,56] that its variance is minimal since, unlike the Gaussian noise, it receives no contribution from the diagonal matrix elements of the quark propagator.

Complex Z_2 (or Z_4) has been adopted in many quark loop calculations [57–60] and the stochastic estimation of determinants [61]. However, the volume Z_2 noise is not a good estimator for connected insertion calculation where the hadron correlator $C(t, 0)$ is needed for large time separation. In this case, the signal falls off exponentially ($C(t, 0) \sim e^{-mt}$), yet the variance decreases only as the inverse power of the noise number [55]. To alleviate this difficulty, dilution of the noise is suggested so that the noise is applied to one time slice at a time and supplemented with low-mode substitution [23,24].

In the following, we shall consider the Z_3 noise which can be used for baryons as well as mesons.

1. Signal-to-noise ratio

We should first remark that the noise wall source, by itself, does not reduce errors as compared to the point source. To see this, we shall consider the variance of the meson and baryon correlators. Besides the large time behavior first considered by Lepage [62], there are prefactors associated with the noise source. The meson correlator in Eq. (13) with a noise wall source has the following behavior at large t,

$$C_M(t, \vec{p} = 0) \sim V_3 e^{-m_M t}, \qquad (33)$$

where V_3 is the three-volume of the noise with its support on a time slice. This comes from the noise estimate with $\sum_{\vec{x}, \vec{y}} \langle \eta^\dagger(\vec{x}) \eta(\vec{y}) \rangle \propto V_3$. Thus, the signal from the noise estimator is larger than that of a point source by a factor of V_3 according to our normalization convention of the noise. On the other hand, the variance of the correlator at large t is

$$N\sigma_M^2(t) \approx \langle G_M(t)^2 \rangle - \langle G_M(t) \rangle^2, \qquad (34)$$

where $N = N_g \times N_n$ and $G_M(t)$ is the meson propagator in each gauge and noise configuration as defined in terms of the meson correlator in Eq. (13), i.e.

$$C(t) = \langle G_M(t) \rangle. \qquad (35)$$

In the case of the flavor nonsinglet meson, the lowest energy state in the variance correlator of Eq. (34) is about the mass of two pions. The noise from the first term contributes a volume squared factor from the four quark propagator, i.e.

$$\sum_{\vec{x}, \vec{y}, \vec{x}', \vec{y}'} \langle \eta^\dagger(\vec{x}) \eta(\vec{y}) \eta^\dagger(\vec{x}') \eta(\vec{y}') \rangle \propto V_3^2. \qquad (36)$$

Therefore, at large t

$$\sigma_M(t) \approx \frac{V_3}{\sqrt{N}} e^{-m_\pi t} \qquad (37)$$

The signal-to-noise ratio is

$$\frac{C_M(t, \vec{p} = 0)}{\sigma_M(t)} \approx \sqrt{N} e^{-(m_M - m_\pi)t}. \qquad (38)$$

The volume factor cancels out and there is no gain in statistics with the noise wall source as compared to a point source. For the pion correlator, the signal-to-noise ratio is nearly constant at large t as noted before [62].

The baryon case is different. Consider the nucleon correlator which has the generic form

$$C_N(t, \vec{p} = 0) \sim \langle S(t, 0)S(t, 0)S(t, 0) \rangle, \qquad (39)$$

where $S(t, 0)$ is the u/d quark propagator and it is produced with a Z_3 wall source. We have suppressed the associated γ matrices in this expression. At large t,

$$C_N(t, \vec{p} = 0) \approx V_3 e^{-m_N t}. \qquad (40)$$

The V_3 factor comes from the sum of the noises at the source end,

$$\sum_{\vec{x}, \vec{y}, \vec{z}} \langle \eta(\vec{x}) \eta(\vec{y}) \eta(\vec{z}) \rangle = V_3. \qquad (41)$$

As for the variance

$$N\sigma_N^2(t) \approx \langle S^3(t, 0)S^{\dagger 3}(t, 0) \rangle - C_N^2(t, 0), \qquad (42)$$

the lowest mass state in the first term at large t is 3 pions which is lower than that of the second term which falls off like $e^{-2m_N t}$. Besides the large time behavior, the variance has a prefactor from the noise

$$\sum_{\vec{x}, \vec{y}, \vec{z}, \vec{x}', \vec{y}', \vec{z}'} \langle \eta^\dagger(\vec{x}) \eta^\dagger(\vec{y}) \eta^\dagger(\vec{z}) \eta(\vec{x}') \eta(\vec{y}') \eta(\vec{z}') \rangle \propto V_3^3, \qquad (43)$$

so that the signal-to-noise ratio is

$$\frac{C_N(t, \vec{p} = 0)}{\sigma_N(t)} \approx \sqrt{\frac{N}{V_3}} e^{-(m_N - 3/2m_\pi)t}. \qquad (44)$$

It shows that, besides the familiar large time fall off, there is an additional factor of $V_3^{-1/2}$ due to the noise. This makes the Z_3 wall source worse than the point source statistically.

To illustrate the above analysis numerically, we show the relative errors of the pseudoscalar, vector, and nucleon correlators from the Wilson fermion ($\kappa = 0.154$ which corresponds to the strange quark mass) on 100 quenched Wilson gauge configurations ($\beta = 6.0$) with one Z_3 wall source. As shown in Fig. 10, the relative errors for the pion [Fig. 10(a)] is about the same as that for a point source which tends to level off in the range $t = [7, 11]$ as expected. For the ρ [Fig. 10(b)] and nucleon [Fig. 10(c)], we observe that, in addition to the expected rise of noise-to-signal ratio at large t, the Z_3 wall source result is worse for the ρ and much worse for the nucleon than those of the point source (N.B.; the scales for the ordinates are different in the three subgraphs.) This is consistent with the extra $1/\sqrt{V_3}$ factor in Eq. (44) for the nucleon.

The undesirable large variance of the noise estimate is rooted in the noise contamination from the neighboring sites which goes down slowly with $N_n N_g$ in Eq. (17)
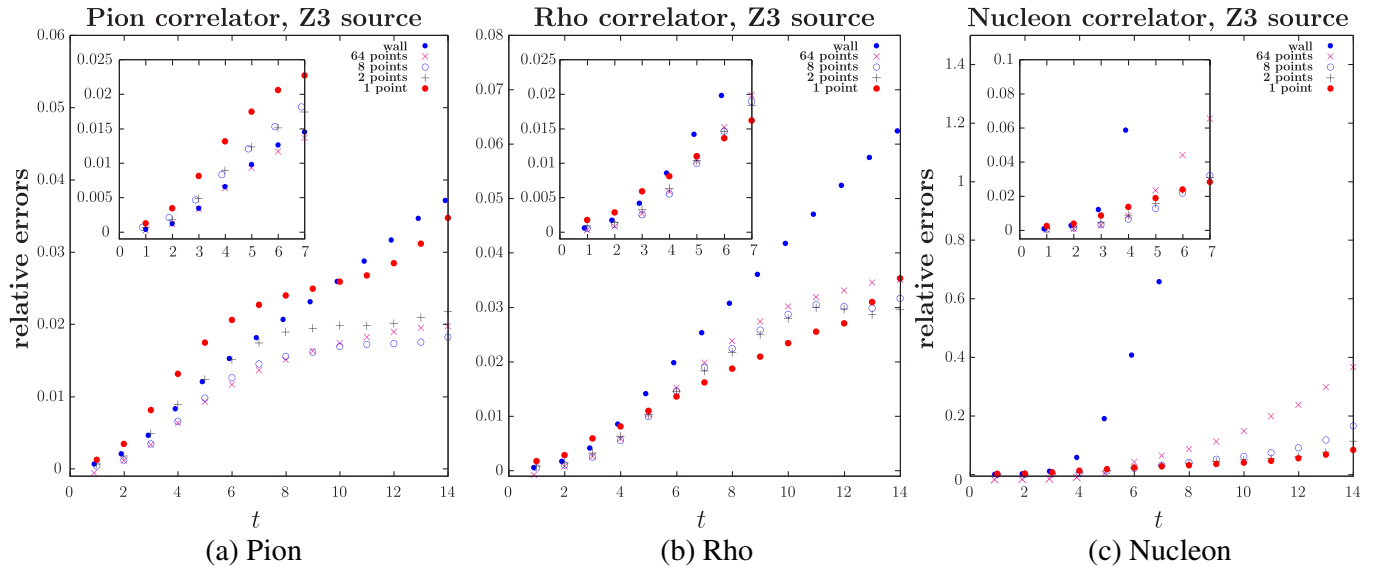
FIG. 10 (color online). Relative errors for (a) Pion, (b) Rho, and (c) Nucleon correlators for different Z_3 sources. These are calculated with Wilson fermion with $\kappa = 0.154$ and $\beta = 6$.

because σ_n is more than an order of magnitude larger than σ_g [28]. To alleviate this difficulty, unbiased subtraction of contamination from the neighboring sites has been employed to reduce the variance in the calculation of quark loops [57–61]. In the case of connected insertions, it is found that dilution in time slices [23,24] is effective in reducing contamination from the nearby time slices. To carry the suggestion further, dilution of space points within a time slice should further reduce the variance [63]. To check this idea, we use a Z_3 grid source with support on certain spatial grid points in a time slice to calculate the quark propagator. This we refer to as the Z_3 grid source. The results are also included in Fig. 10. The 64/8 points refers to the points of the grid which are separated by 4/8 lattice spacings in each spatial direction on a time slice of the $16^3 \times 24$ lattice. We first observe that they are all better than the Z_3 wall source. In the case of pion, they are even better than the point source at large t. For ρ and nucleon, it is interesting to note from the inserts in Fig. 10(b) and 10(c) that the relative errors of Z_3 grids are smaller than those of the point source roughly in the time ranges which are smaller than the corresponding spatial separations of the grid points. We will return to this point later when we discuss heavy quarks.

2. Low-mode substitution (LMS)

From the above study, we conclude that the noise grid source itself does not improve the statistics of the hadron correlators over the point source except for the pseudoscalar meson. Next, we shall consider low-mode substitution. Since the meson correlators at large time separation are dominated by the low-energy modes, substituting the low-frequency part of the noise estimated correlator C_{LL} with the exact one $\tilde{C}_{LL}$ from the eigenmodes, as is outlined in

Eq. (18), has been shown to reduce the variance [22–24]. However, the contributions from hadrons on different sites of the source time slice are correlated, particularly among the nearby neighbors. To see how correlated they are, we plot the relative errors of $\tilde{C}_{LL}$ at large time separation for the wall source as well as the grid sources with 1, 8, 64, 128, 256, and 512 grid points.

These grid points are spaced uniformly in each spatial direction on the source time slice. Plotted in Fig. 11 are relative errors for the pseudoscalar, vector, and axial-vector mesons at a quark mass which corresponds to a pion mass $\sim$200 MeV. These are calculated from the 400 pairs of eigenmodes from 50 $32^3 \times 64$ DWF lattice configurations with $m_l = 0.004$. We see that the relative errors are practically the same from the whole wall down to 64 grid points. This shows that there is no practical advantage to use the noise wall source, since the low-mode contributions from mesons emerging from different sites are highly correlated. $\tilde{C}_{LL}$ would be the same with as little as 64 grid points.

We have learned that if the grid points are too dense, such as close to that of the wall, there is large noise contamination from the neighboring sites. On the other hand, the low-mode substituted part of the correlator $\tilde{C}_{LL}$ is highly correlated among neighboring points. Thus, the clear choice is to reduce the wall source to a grid source with an optimal separation between the grid points to reduce noise contamination and, at the same time, not to sacrifice the variance reduction from low-mode substitution and the gain in statistics with multiple grid points. This would be a many-to-all approach as opposed to the all-to-all approach. It may not make much of difference for the pion, but is expected to work better for other mesons and the baryons. This optimal choice of grid points on a lattice could depend on the number of eigenmodes and perhaps
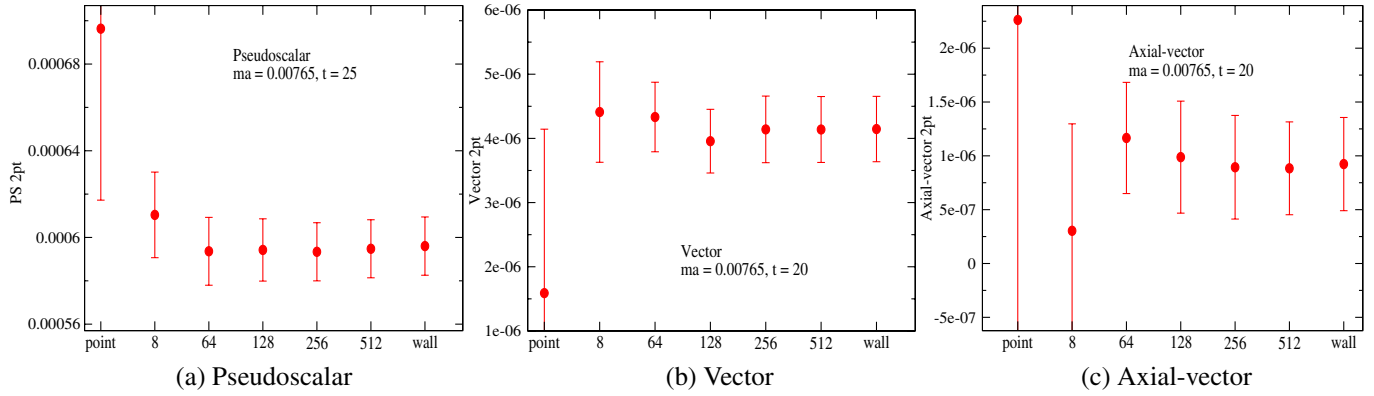
FIG. 11 (color online).   Relative errors from the low-frequency modes at large t separation ($t = 25$ for the pseudoscalar meson and $t = 20$ for the vector and axial-vector mesons) with different number of grid points.

the hadrons, such as mesons vs baryons, in addition to the balance between high- and low-modes. We have not done a detailed analysis in this regard. We shall, nevertheless, present results based on 50 DWF configurations on the $32^3 \times 64$ lattice ($m_l = 0.004$) with a Z_3 grid source, which has support on 64 points (4 points in each spatial direction with 8 lattice spacings apart), and low-mode substitution with 400 pairs of low-frequency modes plus the zero modes.

We first plot in Fig. 12(a) the pseudoscalar correlators from the point source, the Z_3 grid source with 64 grid points, and the Z_3 grid source with low-mode substitution for the case with pion mass at ~200 MeV. Also plotted in Fig. 12(b) are their respective relative errors as a function of t. We see that the relative errors of the Z_3 grid source with or without low-mode substitution is about a factor of

3 smaller than that of the point source in practically all the time range.

A similar situation exists for the strange quark. The results with pseudoscalar mass at ~670 MeV are plotted in Fig. 13.

The case for the charm quark is different. We see in Fig. 14(a) for the quark mass around the charm, that the correlator from the Z_3 grid source with low-mode substitution levels off for $t \geq 12$ and its relative error becomes larger those that of the point and the Z_3 grid sources for $t \geq 7$. This is the classic example where the signal falls off exponentially and the noise estimate levels off at some stage due to a constant variance. In this case, the results from the low-mode substitution will not be useful. On the other hand, we notice that the error from the Z_3 grid is about a factor of 3 smaller than that of the point source at
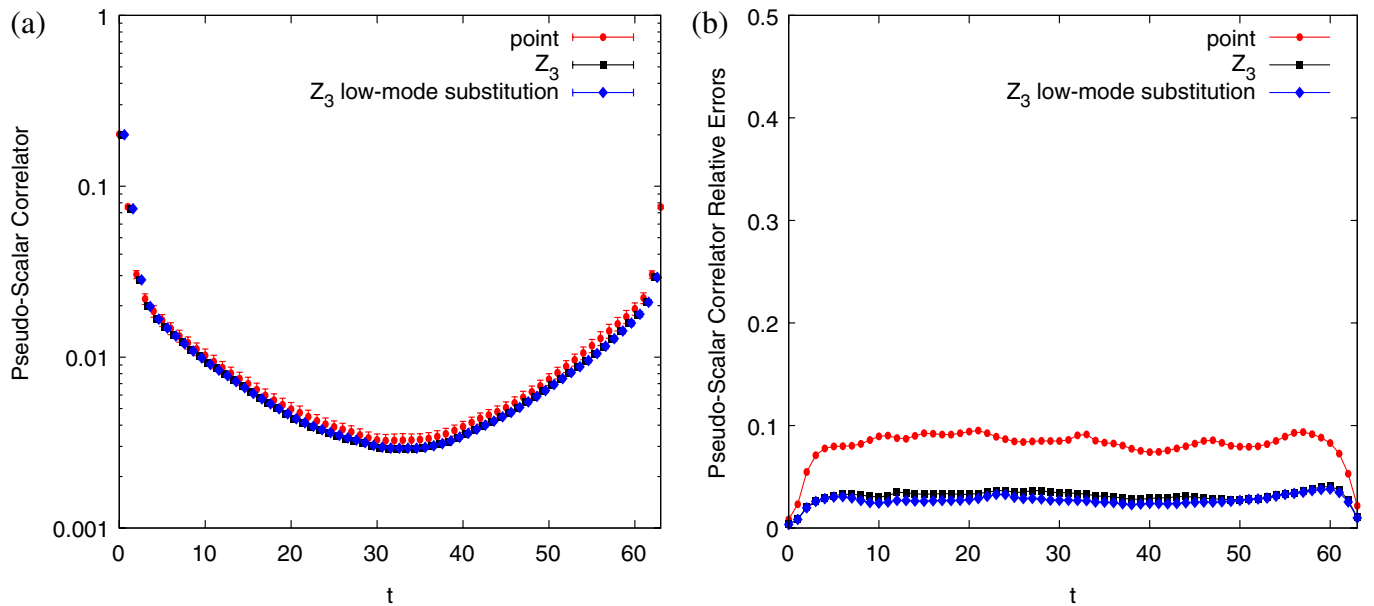

FIG. 12 (color online).   (color online) (a) The pseudoscalar meson correlators from the point (circle), the Z_3 grid source with 64 grid points (square) and the Z_3 grid source with low-mode substitution (diamond) are plotted as a function of t. (b) The respective relative errors are plotted as a function of t.
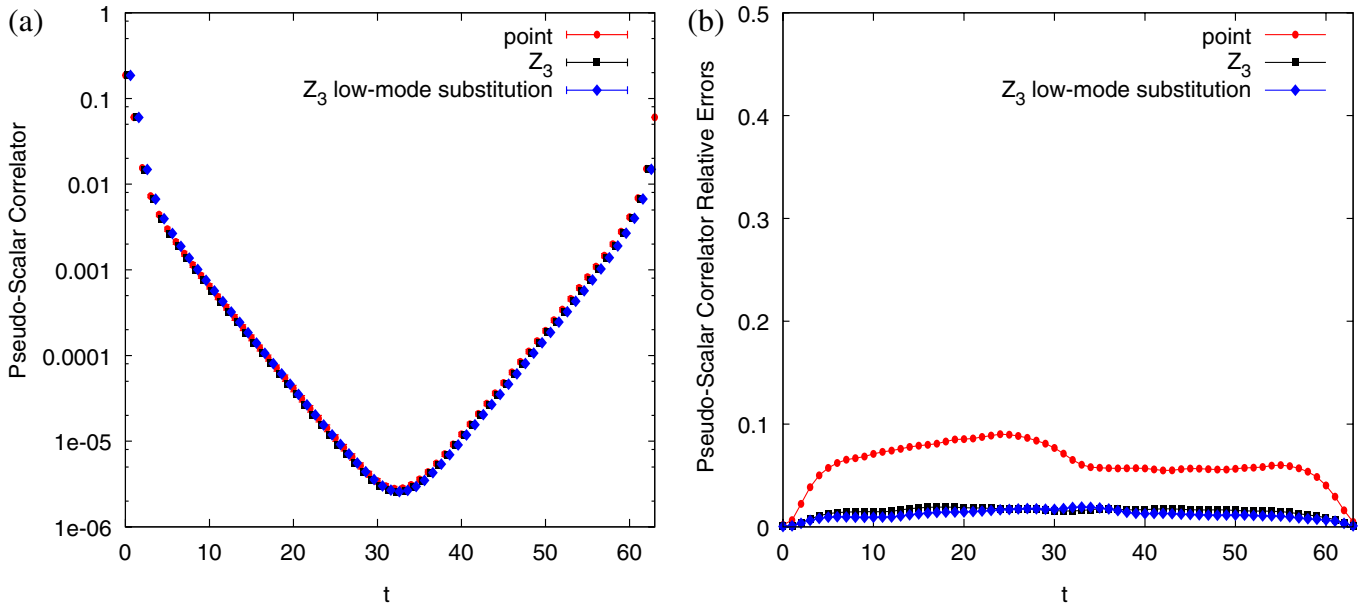
FIG. 13 (color online).   (color online) The same as Fig. 12 for the strange quark mass corresponding to pseudoscalar mass at ~670 MeV.

large t which resembles the situation with the low-mode substitution for the light quarks when the time separation is less than that of the spatial separation of the grid points. It is interesting to ponder why this is so. Although without a proof, we venture to speculate that since the quarks are confined and the charm quark velocity v is about 30% of the speed of light, spatial separation Δx of two grid points greater than v times the Euclidean time separation Δt, i.e. $\Delta x > v \Delta t$, is "space like" in the Minkowski space sense, and that would limit the interference of the two sources.

For the minimal spatial separation of 8 lattice spacings, this limiting Δt is 27 which is close to the mid point of the time extent of 64. This is consistent with what we observed earlier for the light quarks that the relative errors of Z_3 grids are smaller than those of the point source roughly in the time range shorter than the spatial minimal separation of the grid points. In that case, the light quarks are expected to propagate close to the speed of light.

In the case of the vector meson, we see in Fig. 15 that for light quark mass ($m_\pi \sim 200$ MeV), the relative error due
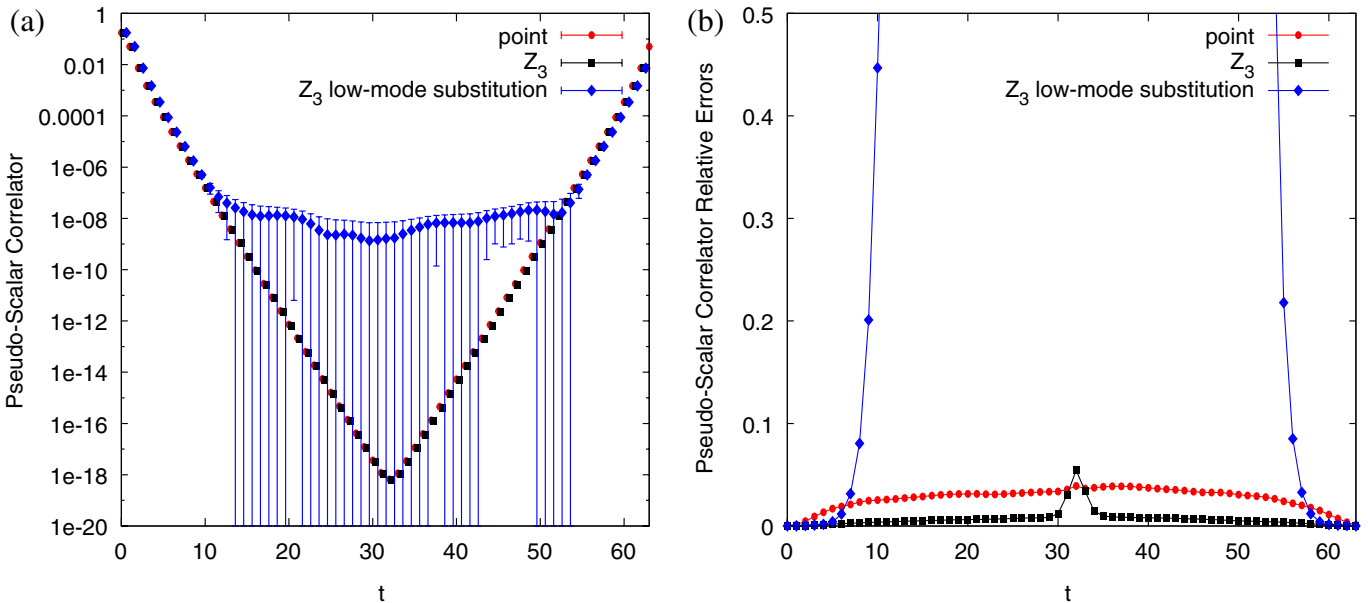

FIG. 14 (color online).   (color online) The same as Fig. 12 for the charm quark mass corresponding to pseudoscalar mass at ~2979 MeV.
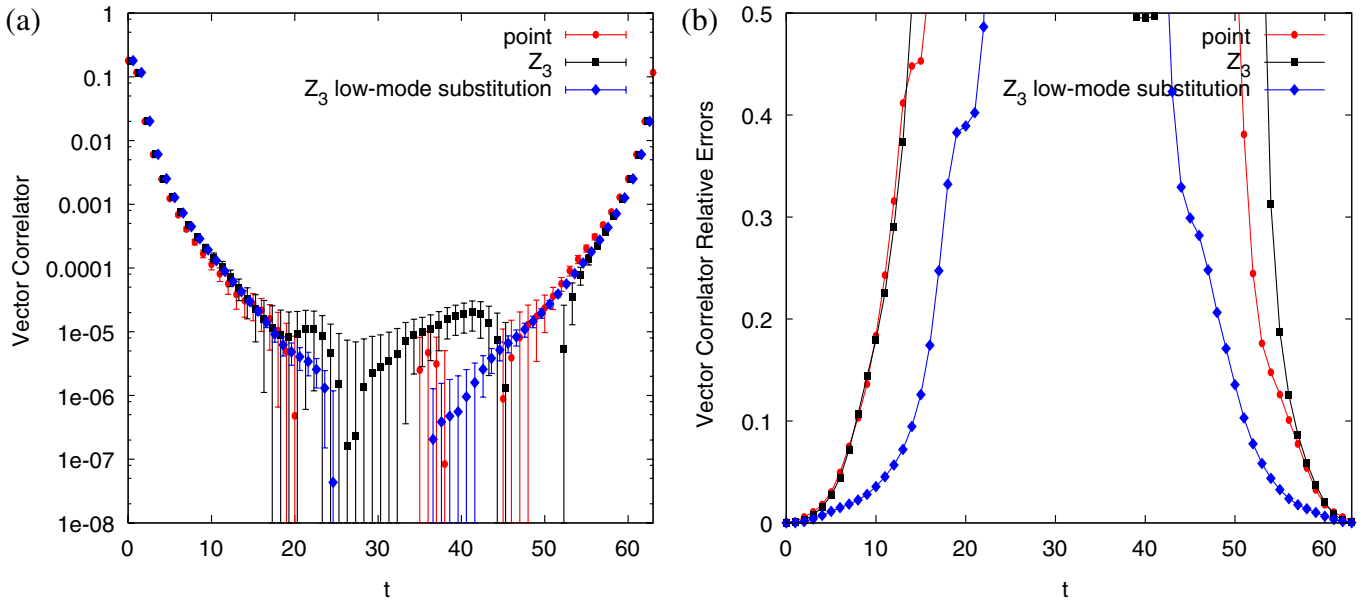
FIG. 15 (color online).   (color online) The same as Fig. 12 for the vector meson correlator with light quark ($m_\pi \sim 200$ MeV.)

to the Z_3 grid source with LMS is a factor of 4 to 5 times smaller than those of the point and the grid sources. For the strange quark mass region (Fig. 16), the LMS has smaller relative error in the range $t < 22$ and then the error becomes larger than those of the point and the grid sources beyond this range. The charm quark case in Fig. 17 is similar to that of the pseudoscalar meson in Fig. 14. Although we do not show them here, the axial and scalar meson correlators are similar to the vector meson case.

We plot the results of the nucleon in Fig. 18 for the quark mass which has a pion mass at ~300 MeV. The left half of

the time range is the nucleon channel and the right half is the S_{11} channel. For the nucleon, we see that the relative error of the grid source becomes larger than that of the point source at $t \sim 7$ which is again close to the 8 lattice spacing separation of the grids. The points labeled by $Z_3\ LLL$ are those with LMS for all three quarks. $Z_3\ LLL + HLL$ represents those with LMS for two quarks in addition to $Z_3\ LLL$. They are defined in Eq. (21). We observe that the error from $Z_3\ LLL$ is smaller than those of the point and grid sources. This reverses the situation where the Z_3 grid source itself is worse than the point
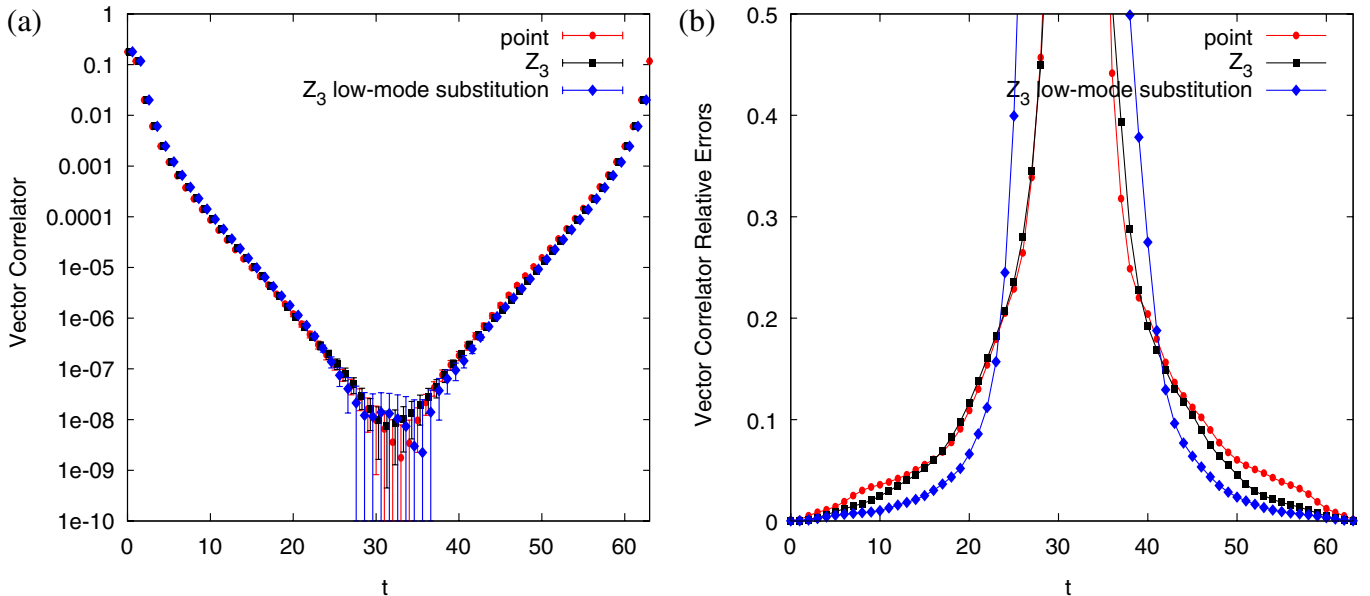

FIG. 16 (color online).   (color online) The same as Fig. 13 for the vector meson correlator with strange quark mass corresponding to pseudoscalar mass at ~670 MeV.
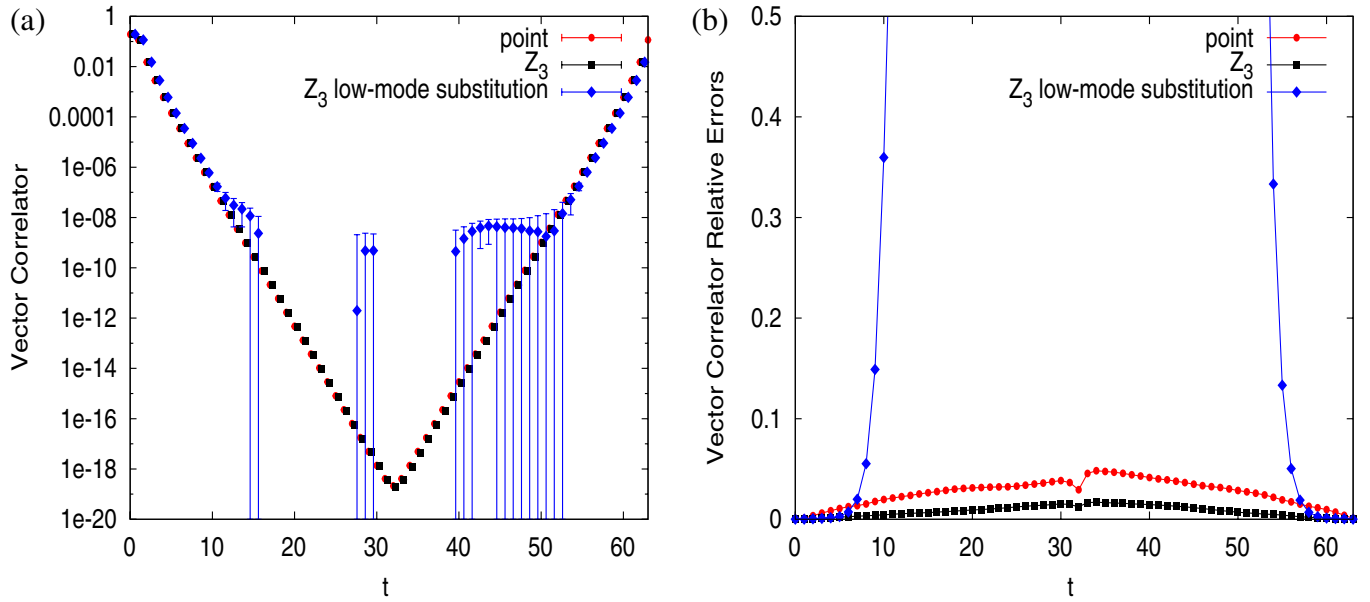
FIG. 17 (color online).   (color online) The same as Fig. 14 for the vector meson correlator with the charm quark mass corresponding to pseudoscalar mass at ∼2979 MeV.
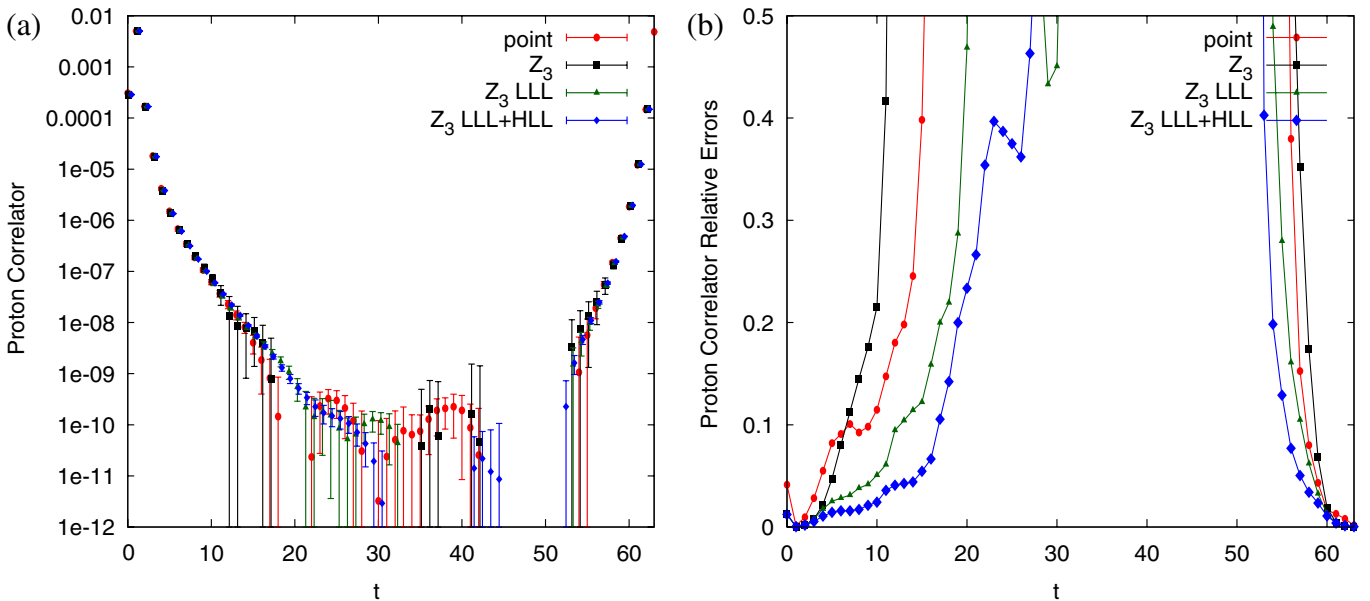

FIG. 18 (color online).   (color online) The same as Fig. 12 for the nucleon correlator with quark mass corresponding to pseudoscalar mass at ∼300 MeV.

source as we remarked before. With more LMS from Z_3 $LLL + HLL$, the relative error is further reduced and is brought down below that of the point source by more than a factor of 4 at large time separation.

V. SUMMARY

To summarize, we have carried out a study of calculating overlap fermion propagators and hadron correlators on the 2 + 1 flavor domain-wall fermion configurations on $16^3 \times 32$, $24^3 \times 64$, and $32^3 \times 64$ lattices with both

deflation in the inversion and low-mode substitution in constructing the correlators.

With HYP smearing and low-mode deflation, we find a speed up from ∼23 for the $16^3 \times 32$ lattice with 200 pairs of eigenmodes and *sim* 51 for the $24^3 \times 64$ lattice with 200 pairs of eigenmodes to ∼79 for the larger $32^3 \times 64$ lattice with 400 pairs of eigenmodes. The cost of the overhead for calculating eigenmodes is 4.5, 4.9 and 7.9 propagators for the above lattices, respectively, which will be amortized with calculation of propagators for more sources. We have

calculated the quark mass dependence of the hyperfine splitting and find that one can accommodate charm quarks with small $O(m^2a^2)$ error. Since this is a mixed-action approach with overlap on DWF sea, we use the finite volume boundary condition property of the scalar correlator to estimate the low-energy constant Δ_{mix} for finite lattice spacing which is needed for the mixed-action partially quenched chiral perturbation theory extrapolation to the physical point and the continuum limit. The preliminary result of $\Delta_{mix} \sim (427 \text{ MeV})^4$ turns out to be small. It only shifts the 300 MeV mixed valence-sea pion mass by ~ 10 MeV at $a^{-1} = 2.32$ GeV for the $32^3 \times 64$ lattice and ~ 19 MeV at $a^{-1} = 1.73$ GeV for the $24^3 \times 64$ lattice.

We have examined the signal-to-noise issue for the connected hadron correlators from the noise source on a time slice and found that the noise wall source is worse than the point source for all mesons except the pion. It is worse still for the baryon (and multiquark systems) by a $\sqrt{V_3}$ factor where V_3 is the 3-volume of the time slice. The situation can be ameliorated by reducing the contamination from neighboring sites with less source points. This introduces the idea of a noise grid source with support on some uniformly spaced grid points on a time slice. On the other hand, we find that the low-frequency part of the multiple hadron source with exact eigenmodes is highly correlated so that, beyond 64 grid points on a time slice of the $32^3 \times 64$ lattice, the relative errors of the meson correlators do not decrease. These observations led to a suggestion of a new algorithm for the grid noise with low-mode substitution to reduce the variance from noise contamination while addressing the low-mode correlation at the same time.

We decide to use 64 Z_3 grid noise and low-mode substitution with 400 pairs of eigenmodes on the $32^3 \times 64$ lattice with the light sea mass $m_l = 0.004$ to calculate both the meson and baryon correlators. We find that for light quarks (pion masses at 200–300 MeV), the errors of the mesons and nucleon masses can be reduced by a factor

of ~ 3 to 4 as compared to the point source. In the strange quark region, the statistical errors of the pion and nucleon masses can be improved by a factor ~ 3, but it is not much improved for the vector meson. We find that the results from low-mode substitution start to degrade beyond the strange quark region. This is due to the fact that the signal falls off quickly at large t and yet the variance of the noise estimation of the high-frequency and the mixed high- and low-frequency parts of the correlator does not fall. Luckily, the Z_3 grid results are still better than the point source and can reduce the errors of the charmonium masses by a factor of ~ 3. One can use it to address the hadrons involving the charm quark. We should point out that the interplay between the noise grid source and low-mode substitution is quite general and is not restricted to a particular fermion action.

So far the study of two-point functions has been favorable. The three-point function with Z_3 grid source and low-mode substitution will undoubtedly pose a different set of challenges.

ACKNOWLEDGMENTS

[1] C. Allton *et al.* (RBC and UKQCD Collaborations), Phys. Rev. D **76**, 014504 (2007).
[2] C. Allton *et al.* (RBC and UKQCD Collaborations), Phys. Rev. D **78**, 114509 (2008).
[3] R. Mawhinney (RBC and UKQCD Collaborations), Proc. Sci., LAT2009 (2009) 081.
[4] T. Blum *et al.*, Phys. Rev. D **66**, 014504 (2002).
[5] J. B. Zhang, N. Mathur, S. J. Dong, T. Draper, I. Horváth, F. X. Lee, D. B. Leinweber, K. F. Liu, and A. G. Williams, Phys. Rev. D **72**, 114509 (2005).
[6] T. DeGrand and Z. Liu, Phys. Rev. D **72**, 054508 (2005).
[7] Y. Chen, S. J. Dong, T. Draper, I. Horváth, F. X. Lee, K. F. Liu, N. Mathur, and J. B. Zhang, Phys. Rev. D **70**, 034502 (2004).
[8] S. J. Dong and K. F. Liu, Proc. Sci., LAT2009 (2009) 090.
[9] R. G. Edwards, G. T. Fleming, Ph. Hagler, J. W. Negele, K. Orginos, A. V. Pochinsky, D. B. Renner, D. G. Richards, W. Schroers (LHPC collaboration) Phys. Rev. Lett. **96**, 052001 (2006).
[10] C. Allton, C. Maynard, A. Trivini, and R. Tweedie, Proc. Sci., LAT2006 (2006) 202.
[11] S. Dürr *et al.*, Proc. Sci., LAT2007 (2007) 113.

[12] K. Cichy, G. Herdoiza, and K. Jansen, Acta Phys. Polon. Supp. **2**, 497 (2009).arXiv:0910.0816

[13] H. Neuberger, Phys. Lett. B **417**, 141 (1998).

[14] For a review, see W. Wilcox, Proc. Sci., LAT2007 (2007) 025.

[15] R. Edwards, U. Heller, and R. Narayanan, Nucl. Phys. B **540**, 457 (1999).

[16] S. J Dong, F. X. Lee, K. F. Liu, and J. B. Zhang, Phys. Rev. Lett. **85**, 5051 (2000).

[17] R. Morgan and W. Wilcox, arXiv:0707:0505.

[18] A. Stathopoulos and K. Orginos, arXiv:0707.0131.

[19] M. Lüscher, J. High Energy Phys. 07 (2007) 081.

[20] H. Neff, N. Eicker, T. Lippert, J. W. Negele, and K. Schilling, Phys. Rev. D **64**, 114509 (2001).

[21] L. Venkataraman and G. Kilcup, Nucl. Phys. B, Proc. Suppl. **63**, 826 (1998).

[22] T. DeGrand and S. Schaefer, Comput. Phys. Commun. **159**, 185 (2004).

[23] J. Foley, K. J. Juge, A. O'Cais, M. Peardon, S. M. Ryan, and J. Skullerud, Comput. Phys. Commun. **172**, 145 (2005).

[24] T. Kaneko, H. Fukaya, S. Hashimoto, H. Matsufuru, J. Noaki, T. Onogi, and N. Yamada (JLQCD collaboration), Proc. Sci., LAT2007 (2007) 148.

[25] M. Lüscher, Phys. Lett. B **428**, 342 (1998).

[26] K. F. Liu and S. J. Dong, Int. J. Mod. Phys. A **20**, 7241 (2005).

[27] W. Wilcox and B. Lindsay, Nucl. Phys. B, Proc. Suppl. **63**, 973 (1998).

[28] M. Deka, T. Streuer, T. Doi, S. J. Dong, T. Draper, K. F. Liu, N. Mathur, and A. W. Thomas, Phys. Rev. D **79**, 094502 (2009).

[29] J. van den Eshof et al., Comput. Phys. Commun. **146**, 203 (2002); Nucl. Phys. B, Proc. Suppl. **106-107**, 1070 (2002).

[30] A. Hasenfratz and F. Knechtli, Phys. Rev. D **64**, 034504 (2001).

[31] S. Dürr, C. Hoelbling, and U. Wenger, J. High Energy Phys. 09 (2005) 030.

[32] S. Aoki et al. (PACS-CS Collaboration), Phys. Rev. D **81**, 074503 (2010).

[33] K. F. Liu and C. W. Wong, Phys. Lett. B **73**, 223 (1978).

[34] S. J. Dong and K. F. Liu, Proc. Sci., LAT2007 (2007) 093.

[35] T. G. Kovacs, Phys. Rev. D **67**, 094501 (2003).

[36] H. Leutwyler and A. V. Smilga, Phys. Rev. D **46**, 5607 (1992).

[37] T. Blum et al., Phys. Rev. D **69**, 074502 (2004).

[38] S. J. Dong, T. Draper, I. Horvath, F. X. Lee, K. F. Liu, and J. B. Zhang, Phys. Rev. D **65**, 054507 (2002).

[39] O. Bar, G. Rupak, and N. Shoresh, Phys. Rev. D **67**, 114505 (2003); **70**, 034508(E) (2004).

[40] O. Bar, C. Bernard, G. Rupak, and N. Shoresh, Phys. Rev. D **72**, 054502 (2005).

[41] J. W. Chen, D. O'Connell, and A. Walker-Loud, J. High Energy Phys. 04 (2009) 090.

[42] M. Golterman, T. Izubuchi, and Y. Shamir, Phys. Rev. D **71**, 114508 (2005).

[43] S. Prelovsek, Phys. Rev. D **73**, 014506 (2006).

[44] C. Aubin, J. Laiho, and R. S. Van de Water, Phys. Rev. D **77**, 114501 (2008).

[45] A. Walker-Loud et al., Phys. Rev. D **79**, 054502 (2009).

[46] C. Aubin and C. Bernard, Phys. Rev. D **73**, 014515 (2006).

[47] B. Tiburzi, Phys. Rev. **72**, 094501 (2005).

[48] J. W. Chen, D. O'Connell, and A. Walker-Loud, Phys. Rev. D **75**, 054501 (2007).

[49] K. Orginos and A. Walker-Loud, Phys. Rev. D **77**, 094505 (2008).

[50] S. Dürr et al., Proc. Sci., LAT2007 (2007) 115.

[51] W. Detmold, K. Orginos, M. J. Savage, and A. Walker-Loud, Phys. Rev. D **78**, 054514 (2008).

[52] S. Prelovsek and D. Mohler, Phys. Rev. D **79**, 014503 (2009).

[53] S. Prelovsek, T. Draper, C. B. Lang, M. Limmer, K.-F. Liu, N. Mathur, and D. Mohler, arXiv:1005.0948.

[54] T. Draper, T. Doi, K. F. Liu, D. Mankame, N. Mathur, and X. Meng (χQCD Collaboration), Proc. Sci., LAT2008 (2008) 108.

[55] S. J. Dong and K. F. Liu, Phys. Lett. B **328**, 130 (1994).

[56] S. Bernardson, P. McCarty, and C. Thron, Comput. Phys. Commun. **78**, 256 (1994).

[57] S. J. Dong, J.-F. Lagaë, and K. F. Liu, Phys. Rev. Lett. **75**, 2096 (1995).

[58] S. J. Dong, J.-F. Lagaë, and K. F. Liu, Phys. Rev. D **54**, 5496 (1996).

[59] S. J. Dong, K. F. Liu, and A. G. Williams, Phys. Rev. D **58**, 074504 (1998).

[60] T. Doi, M. Deka, S. J. Dong, T. Draper, K. F. Liu, D. Mankame, N. Mathur, and T. Streuer, Phys. Rev. D **80**, 094503 (2009).

[61] C. Thron, S. J. Dong, K. F. Liu, and H. P. Ying, Phys. Rev. D **57**, 1642 (1998).

[62] G. P. Lepage, Proceedings of TASI'89: From Actions to Answers, (Boulder ASI, Boulder 1989), 97.

[63] We thank R. Edwards for the suggestion.